Marie Skłodowska-Curie Actions

This project has received funding from the European Union's Horizon 2020 research and innovation programme under the Marie Skłodowska-Curie grant agreement No. 642453

Training in Reducing Uncertainty in Structural Safety

D4.2 Final Report

WP4 - Building, Energy, and Marine Infrastructure

Revision [final version]

Deliverable Number	Deliverable Title	Lead Beneficiary	Type	Dissemination Level	Due date
D4.2	Final Report	NUID UCD	Report	Public	31-Dec-2018

Start Date of the Project: 01-Jan-2015 Duration: 48 months

List of Contributors

The order below is by alphabetical order of the authoring organizations, and has nothing to do with the extent or importance of the contributions. The main contributors to a specific research topic are provided at the start of each chapter.

Aalborg University, Aalborg, Denmark
Michael H. Faber

ARUP, Dublin, Ireland
Md Shah Nur Alam Sourav (ESR2)
Salam Al-Sabah

Burgmann Packings, Dublin, Ireland
Greg Byrne

Equipos Nucleares S.A. (ENSA), Maliaño, Spain
Alberto González Merino (ESR3)
Luis Costas De La Peña

Lloyd's Register EMEA, Southampton, UK
Giulia Milana (ESR6)
Guang Zou (ESR5)
Kian Banisoleiman

Trinity College Dublin (TCD), Dublin, Ireland
Alan O'Connor
Maria Nogal
Rui Teixeira (ESR4)

University College Dublin (UCD), Dublin, Ireland
Arturo González (Project Coordinator)
Ciaran McNally (WP4 leader)
Sofia Antonopoulou (ESR1)

Edited by Arturo González, Ciaran McNally and Parisa Beizaei

Table of Contents

Executive Summary

The EU TRUSS (Training in Reducing Uncertainty in Structural Safety, 2015-2018) ITN (Innovative Training Network) project features 14 Early Stage Researchers (ESRs), each of whom has conducted 3 years of Ph.D. level research on key issues relating to structural reliability (http://trussitn.eu/). Six of these researchers have worked on research topics that fall into WP4: Buildings, Energy and Marine Infrastructure. Although these applications are quite diverse, they are connected by virtue of the very aggressive environments that the infrastructure is subjected to. Some of these are corrosive, others are radioactive, and all display non-linear structural responses. They also bring together relatively high uncertainties regarding material properties and modelling. The individual research projects can be further sub-divided into 3 categories based on their areas of application. These are:

- **Materials and Buildings** (ESR1,ESR2)
  - Uncertainty in material strength is addressed via complex materials characterization and subsequent reliability assessment of the developed braided Fiber Reinforced Polymer (FRP).
  - Assessment and testing of concrete strength of existing structures, through the development of a novel pull-out test.
- **Energy Infrastructure** (ESR3,ESR4)
  - Uncertainty in the design of energy infrastructure is addressed using complex response models for freestanding nuclear-spent fuel racks.
  - Development of probabilistic optimisation tools for the fatigue design of Offshore Wind turbine Towers (OWT).
- **Infrastructure in a Marine Environment** (ESR5,ESR6)
  - Novel maintenance strategies for optimising the residual life of ageing marine structures subject to fatigue loading, based on probabilistic fracture mechanics.
  - Understanding the fatigue behaviour of ship unloaders, using monitored data to provide estimations of residual service life.

An ESR has been conducting research in each of these topics under the supervision of TRUSS academic and industrial experts. After 36 months, each ESR submitted or was in the process of submitting a related Ph.D. thesis. A brief summary of their projects is now provided.

In *Chapter 1*, Sofia Antonopoulou (ESR1) investigates the performance of braided FRP as a structural reinforcement. Her work is focused on understanding the behaviour of braided basalt FRP bars designed for internal concrete reinforcement. Working with an industry partner (Burgmann Packings), she designs and manufactures a large number of rebar types. These are investigated through a combination of numerical analysis, visual assessment, and experimental work. Her numerical analysis is based on classical laminate theory and highlights the significant influence of geometric design on the properties of the final design. Bars are then manufactured based on this analysis and characterised based on their tensile test and modulus of elasticity. Visual assessment using a digital microscope is used for initial characterisation, which is later supported by micro CT scanning to provide fundamental information on the influence of porosity on the final performance. Fatigue testing is also conducted to show the potential for her designs when subjected to cyclical loading applications.

The work by Shah Nur Alam Sourav (ESR2) on the in-situ assessment of concrete strength is described in *Chapter 2*. As part of his research, he develops a novel test, called the Post-installed Screw Pull-out (PSP) test. This test aims to improve the reliability of strength assessment in a way that is cost-effective, quick, and relatively non-destructive. His experimental work shows the PSP test to be reliable and reasonably accurate (compared to other commercially available alternatives, including core testing). This is particularly the case for concretes with softer aggregate. His experimental work is supported by finite element analysis using Abaqus, where he models the interaction between the screw and the surrounding concrete and characterises the failure mechanism. He is validating the test by applying it to concrete on some current civil engineering projects in Dublin. If adopted, this test will ultimately contribute to reducing uncertainty in compressive strength assessment of concrete in existing structures.

Alberto González Merino (ESR3) is concerned with the design of free-standing racks storing spent nuclear fuel. These racks are generally closely spaced and are submerged in a pool to store and cool the nuclear fuel. His research, presented in *Chapter 3*, investigates the accuracy of current analysis methodologies, the robustness of the computed outputs and their sensitivity to a number of selected variables. Implicit assumptions are identified together with the major sources of uncertainty related to input data, and statistical methods for forward uncertainty propagation are applied to a basic 2-rack system. He determines transient envelopes and quantitative response surfaces from simulation experiences in ANSYS Mechanical. A multivariate sensitivity analysis is conducted to assess the influence of the uncertain variables on the numerical outcomes. He then uses Latin Hypercube Sampling for the design of experiments in order to effectively explore the multidimensional input space. Scatter plots of key variables including seismic and fuel loadings, equivalent dynamic properties, friction coefficients, contact stiffnesses, fuel gaps, inertias, time stepping, convergence tolerances, Rayleigh damping, etc., are derived. Sobol index and variance-based importance factors are obtained from surrogate models and computed through Polynomial Chaos Expansions. Finally, a safe design point with the highest probability of failure is found using reliability methods. Based on the findings, significant recommendations and enhancements of the analysis methodologies are proposed.

The probabilistic optimisation of towers for offshore wind turbines is the objective of Rui Teixeira (ESR4) in *Chapter 4*. His research offers new insights into the operational design for offshore wind turbines and its probabilistic assessment. For extrapolation of significant wave heights, results of the Goodness-of-Fit analysis and extrapolation show that there is no evidence to reject the Generalised Pareto distribution over

the two-parameter Weibull and the Exponential distributions. In the case of S-N fatigue assessment, accurate long-term estimations are seen to depend mainly on the short-term damage estimation loading sample for S-N fatigue calculations. Global sensitivity analysis is identified to be a powerful tool to decrease the cost needed to solve an engineering problem. Within a complex problem, it is common for only a limited number of variables to comprise for almost all the influence in the problem's output. A meta-modelling technique, using a Kriging surrogate, is successfully implemented in order to reduce the computational time of OWT S-N fatigue design significantly.

Chapter 5 covers the contributions in integrity management of ship structures by Guang Zou (ESR5). Welded structural systems are susceptible to fatigue primarily due to the presence of initial flaws. Structural reliability against fatigue and fracture failures are lifetime considerations which require decisions on plate thickness, allowable stress range, welding quality assurance procedure, inspection intervals, repair method, etc. It is a current practice that the structural fatigue design and structural integrity management are generally disconnected. This means that integrity management optimization has not received due consideration in the design stage, and integrity management optimization is done at the operational stage when the structural plan cannot be changed. The research by ESR5 offers a holistic perspective and develops a risk-based method for jointly optimizing design and maintenance plans for structures subjected to fatigue. The method is built upon probabilistic modelling of fatigue damage accumulation, crack growth, inspection quality, and effect of repair. The method can also model the combined effects of structural geometry and maintenance strategy on the lifetime fatigue reliability and costs.

Finally, *Chapter 6* addresses structural assessment of ship unloaders through the research by Giulia Milana (ESR6). For these structures, fatigue plays a critical role in service life assessment, and accurate evaluations of fatigue life are particularly important. Her research makes use of data acquired from a monitored structure, and using the obtained stress ranges, a fatigue life assessment is carried out, based on S-N curves and Miner’s rule for the cumulative damage. A 3D finite element model of the whole ship unloader is developed to estimate the remaining life for each structural element. The residual life in terms of remaining tonnes to be lifted is also determined for the most critical elements of the lifting boom. Developed histograms show that the standard procedure provides a remaining life that is less than half of that obtained introducing a probabilistic approach. The latter suggests that the standard procedure leads to an assessment that is far too conservative, and that a more accurate study of the load applied to the structure and of how unloading cycles are modelled can avoid unnecessary replacements.

The projects described above are quite diverse and have focused on a wide array of structural applications. They have highlighted the need to overcome uncertainty in material and structural performance, and this represents a core thread that ties the projects together. The continued interaction between the researchers involved has enhanced their research, and this is reflected in the quality of the Ph.D. theses that have been submitted or that are currently being finalised.

Chapter 1: Reliability of concrete structures reinforced with braided FRP

Sofia Antonopoulou[1], Ciaran McNally[1], Greg Byrne[2]
[1]School of Civil Engineering, University College Dublin, Dublin, Ireland
[2]Burgmann Packings Ltd, Dublin, Ireland
email: sofia.antonopoulou@ucdconnect.ie, ciaran.mcnally@ucd.ie

ABSTRACT: This project focuses on design, development, and characterisation of Basalt Fibre Reinforced Polymer (BFRP) composites, for internal concrete reinforcement, using braiding as a manufacturing technique. The main goal is to explore their full potential in infrastructure applications through design optimisation and evaluation of their structural performance. Braided BFRP preforms with different configurations are designed and manufactured by changing key braiding parameters in order to achieve the desired structural geometry and to meet the performance characteristics of existing rebar reinforcement. Successful epoxy resin impregnation trials in regular and spiral geometries confirm the possibility of manufacturing braided BFRP composites in complex shapes. Mechanical properties of laboratory manufactured composites are numerically simulated using Classical Laminate Theory (CLT), and tensile tests are then conducted in order to evaluate the analytical data experimentally. A hybrid design approach is also introduced using both braiding technique and unidirectional fibre design to improve the elastic modulus of braided BFRP reinforcement. All rebar types are developed using basalt fibres and epoxy resin as reinforcement and matrix respectively; composites with a constant cross-section of 5, 8, and 10 mm diameter are manufactured using a vacuum assisted resin infusion technique. In addition, micro-computed tomography (μCT) methods and image processing techniques are applied towards a detailed fibre composite material analysis and a precise evaluation of the internal microstructure of BFRP reinforcement. Tensile fatigue tests are performed on selected BFRP designs in order to evaluate their long-term durability. Finally, comparisons are made between different rebar configurations towards the optimisation of the designing and manufacturing process.

KEY WORDS: Basalt Fiber Reinforced Polymer (BFRP) rebars; Braiding; Tensile strength; Fatigue; CT-scanning; FRP characterisation.

1 INTRODUCTION

Degradation of reinforced concrete structures due to corrosion of steel is reported as one of the main causes of structural deficiency that severely affects the structural safety of Reinforced Concrete (RC) elements. Harsh loading conditions and aggressive environmental factors can largely influence the long-term durability of structures in civil engineering applications and eventually lead to undesired repairs, additional costs, and shorter service lives. According to the IMPACT study, published by NACE International in 2016, a total of about $2.5 trillion is currently spent worldwide each year; approaches that have been taken so far, like stainless steel, galvanizing procedures etc., have been found to be unable to successfully address this problem in a cost-effective way [1-3].

In recent years, advanced composite materials, such as BFRP, were introduced as a viable replacement for traditional steel rebars in civil engineering applications. More specifically, these materials can offer significant advantages related to both their non-corrodible nature and their high strength-to-weight ratio. In general, BFRP composites consist of high tensile fibres (i.e., basalt) embedded in polymer matrices (thermosetting or thermoplastic) leading to improved mechanical properties of the system. There are, however, limitations that prevent their use on a larger scale, and lack of ductility is the most significant. The tensile behaviour of FRP rebars is characterized by a linear stress-strain behaviour up to brittle failure; thus a direct substitution between FRP and steel rebars is not feasible. The overall properties and durability of FRPs are strongly dependent on the constituent materials, the composite's fibre and void content, the fibre-matrix interface and the orientation of fibres, which is strongly related to the used manufacturing technique. To date, most of the FRP reinforcement used in concrete has been manufactured by pultrusion, a low-cost method providing composites with a constant cross-section and a smooth surface. This well-known process for manufacturing composites consists of continuously pulling impregnated, formable fibre-reinforcing material through a shaping die where the material is heated and subsequently cured, giving a final uniform cross-sectional shape [4-7].

A detailed investigation of manufacturing technologies and design methodologies for the optimum development of BFRP composites, indicates that braiding methods could provide the required performance benefits through increased ductility and flexibility; it can also enhance the bond between FRP and concrete, which has a direct influence on both the serviceability and the ultimate load-carrying capacity of the structure. The basic principle of the braiding technique is the interlacing of yarns in a way that they cross each other in a diagonal direction. Braiding angle - the angle between braid yarns and the axis of braid structure - is an important parameter that affects mechanical properties of braids and is usually adjusted by changing the take-up speed in the braiding machine, obtaining a range between 20 and 85°. However, braided composites exhibit complex damage and failure behaviour, mainly due to

their textile nature related properties, like multiple curved yarn interfaces, resin rich areas and nesting of different layers. Moreover, combining aspects of pultrusion and braiding into a single manufacturing process can be used to produce a hybrid FRP rebar consisting of both unidirectional and off-axis oriented fibres. The stress-strain behaviour of the composite can be tailored by careful selection of raw materials and architectural design for the core structure and the braided sleeve respectively. The final part is a composite rebar with high initial tensile strength, contributed mostly by the high modulus unidirectional core followed by a gradual failure process associated with the outer braided sleeve [8-12].

Due to the growing interest on the use of FRP composites in construction, a number of design guidelines and standards for their efficient use in civil engineering applications were recently developed by the American Concrete Institute, the Japan Society of Civil Engineers, the British Standards Institution and the Canadian Standards Association International. However, the use of FRP for reinforcement instead of steel is far from widely accepted in the conservative construction industry, mostly because of the lack of familiarity with this material, the high initial costs and the lack of structural ductility. Summarising, the optimum development of a reinforced concrete type in which the usual internal steel rebars are replaced by FRP composite materials is considered to be an ongoing research topic worldwide, but the structural safety associated with this composite material is still not fully understood [12-15].

2 OBJECTIVES

This project aims to assess the reliability of structures manufactured using braided Basalt Fiber Reinforced Polymer (FRP) reinforcement. More specifically, the main goal is to understand the fundamentals in designing and developing BFRP composites for internal concrete reinforcement using braiding as a manufacturing technique and, then evaluate their performance through physical and mechanical characterisation tests.

Reinforcement is designed using basalt fibres and epoxy resin as reinforcement and matrix respectively. Bars are manufactured using braiding, and a vacuum assisted resin infusion technique. Three BFRP rebar sizes with different braided and hybrid configurations are developed and their key characteristics assessed. The relation between geometrical factors and processing conditions on the physical and mechanical properties of the braided rebars is evaluated, allowing assessment of the manufacturing process for improved rebar design. The main objectives can be summarized as follows:

- Design and development of BFRP composites for internal concrete reinforcement using braiding and hybrid manufacturing techniques.
- Full experimental (tensile & fatigue tests) and numerical characterization (CLT approach) of the material.
- Microstructural material analysis using micro-computed tomography (μCT).

The final goal of this project is to explore the potential of braided BFRP reinforcement and encourage their use in civil engineering applications by presenting new and innovative rebar configurations.

3 EXPERIMENTAL WORK

The work conducted so far for this project can be summarised into four separate steps. The first includes the design and manufacture of braided and hybrid BFRP preforms while changing key parameters (angle, nº of layers, etc.). This task takes place exclusively in Burgmann Packings Ltd. Epoxy resin impregnation tests in both regular and spiral configurations using a vacuum assisted resin infusion method (VARIM) for all rebar designs are also completed in SuperTEX Austria, Burgmann Packings Ltd, VEPLAS d.d. and UCD School of Civil Engineering laboratory. During the second step, a theoretical numerical approach based on CLT is developed in UCD to determine the stiffness properties of manufacture BFRP composites, calculating their effective longitudinal in-plane modulus (E_x^{FRP}) and their fibre volume fractions (φ_f). In the third task, the tensile properties of all manufactured BFRP rebars are experimentally determined in UCD School of Civil Engineering laboratory in accordance to B2_ACI 440.3R-04/ ASTM D7205 standard. Then, tensile fatigue performance of selected BFRP designs is experimentally evaluated according to B7_ACI 440.3R-04 standard. Finally, the last step investigates the internal microstructure of all BFRP composite rebars using X-ray micro-computed tomography and image processing techniques at UCD Rosemount Environmental Research Station facilities in order to assess quality and consistency of the manufacturing process and correlate that with their mechanical performance.

3.1 Materials, Designs and Manufacturing Method

Thirteen different types of BFRP composites for internal concrete reinforcement are developed and mechanically characterised within this study; ten fully braided and three hybrid designs. The various raw materials used to develop BFRP rebars are presented in Table 1. Basalt fibres (3 yarns sizes) and epoxy resin are used as reinforcement and matrix respectively. Polyethylene terephthalate (PET) fibres are also used to promote resin flow on samples during the impregnation process [7].

Table 1. Raw material properties.

Product name	Uses	Tensile strength (MPa)	Elastic modulus (GPa)
BASALTEX® - Basalt assembled roving – 300, 600, 2400 tex 13, 17, 19 μm	Fibre reinforcement	2800 – 4800	87 - 89
M183 semi-dull round - PET Monofilament	Impregnation aid	57 – 60	10
Easy Composites - IN2 Epoxy infusion resin/ Slow cure	Resin	65.5 – 73.5	2.95

BFRP preforms in thirteen different sizes and configurations are designed and manufactured in Burgmann Packings Ireland, using (i) a pure braiding technique and (ii) a combined approach with a unidirectional fibre core. In particular, the desired rebar configuration consists of a braided or unidirectional core, one or two layers of PET material to

promote resin flow, and exterior finishing braiding layers to achieve the desired structural geometry. The target is a solid braid of the circular cross-section with a final Outer Diameter (OD) of 5, 8 and 10 mm. A complete BFRP preform along with resin impregnated rebars are presented in Figure 1, while Table 2 lists technical designing details for 5 of the 13 configurations [1,7,12].

Table 2. Technical designing details.

BFRP 1: 5 mm				
Layer	Material	Yarns	OD	Angle
1	300	8	1.6	11
2	300	16	2.7	16
3	PET	32	3.5	9
4	PET	32	4.4	12
5	600	16	5.1	45

BFRP 5: 8 mm				
Layer	Material	Yarns	OD	Angle
1	300	16	2.6	14
2	600	16	4.2	16
3	PET	32	5.0	13
4	PET	32	5.5	14
5	600	16	5.7	34
6	600	16	6.4	34
7	600	24	7.2	31
8	600	24	7.9	38

BFRP 7: 8 mm				
Layer	Material	Yarns	OD	Angle
1	300	8	1.6	12
2	300	16	2.7	16
3	600	16	4.0	17
4	PET	32	4.9	12
5	PET	32	5.6	14
6	300	16	6.5	16
7	600	16	7.2	45
8	600	24	7.9	40

BFRP 8: 10 mm				
Layer	Material	Yarns	OD	Angle
1	300	16	2.6	14
2	600	16	4.2	16
3	PET	32	5.0	13
4	PET	32	5.4	14
5	600	16	6.0	34
6	600	16	6.5	36
7	600	24	7.3	30
8	PET	24	8.0	35
9	600	24	8.8	34
10	600	24	9.8	38

BFRP 11 - 8 mm				
Layer	Material	Yarns	OD	Angle
Core	2400	10	4.4	0
1	PET	24	5.3	30
2	600	8	5.8	45
3	600	8	6.5	45
4	600	12	7.2	45
5	600	12	7.9	45

* Note: All values are an average of readings taken at several locations of manufactured samples; OD: measured (actual) Outer Diameter for each layer (mm); Braid yarns: Basalt (TEX), PET Monofilament; Angle (°).

A vacuum assisted resin infusion method is selected for producing all BFRP specimens. This method involves placing the preform inside the aluminium mould, which is then completely sealed, and immediately after, epoxy resin is infused using a vacuum. A post-curing procedure is then followed to ensure the composite's quality; the rebar is placed in the oven for 6 hours in 60 °C after 24 hours in room temperature environment [7,12].

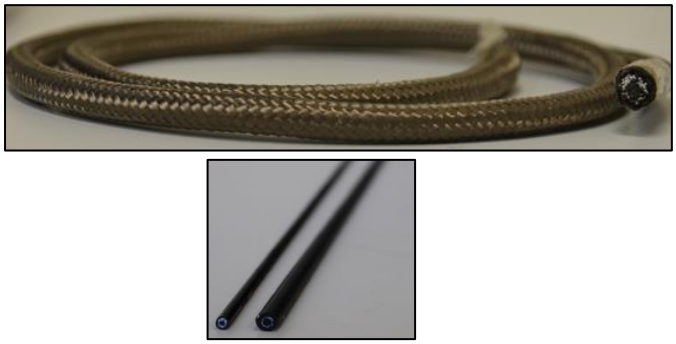

Figure 1. (a) BFRP rebar preform, (b) resin impregnated composite rebars.

3.2 Numerical analysis

A theoretical numerical approach based on CLT is developed to determine the stiffness properties of braided composites, calculating the effective longitudinal in-plane modulus (E_x^{FRP}) and the fibre volume fractions (φ_f) of each braided sample [7,12,16]. For each layer of every BFRP sample, the four independent engineering parameters affecting their stiffness behaviour (longitudinal/ E_x, transverse/ E_y, shear/ E_s modulus and Poisson's ratio/ v) are estimated. Then, the on-axis stiffness matrix [Q_{ij}] for each braid layer is calculated, defining the six off-axis stiffness coefficients along with the braid angle. The stiffness matrix [$A - B - D$] and the cofactor expansion matrix [C] for each BFRP sample can be obtained from terms A_{ij}, D_{ij}, B_{ij}, expressing the extensional, flexural and extensional-bending coupled response respectively. Finally, Equation (1) forms the basis for the evaluation of the elastic properties of braided BFRP rebars:

$$E_x^{FRP} = {DET([A - B - D)]}\Big/{DET([C])} \quad (1)$$

3.3 Mechanical characterisation

3.3.1 Tensile tests

The tensile properties of the manufactured BFRP rebars are determined by testing three representative specimens for each configuration in accordance to B2_ACI 440.3R-04/ ASTM D7205 standard. All tests are performed at room temperature with an Instron 500 Universal Testing Machine of 500 kN capacity, by displacement control and constant loading rate of 1 mm/min. Throughout the whole duration of the test, the applied load, displacement and specimen elongation are electronically recorded. More specifically, an Epsilon 3543-

100M-100M-ST Axial Extensometer (100 mm gauge length) attached on the mid-length position of the rebar is used to track the specimen's elongation. Notched metallic jaws are used in order to align the sample in the testing machine properly. During each test, the specimen should fail in the test section, and slippage should be avoided throughout the length of the anchors, so a special anchoring system is prepared in UCD laboratory; the initial length, L_s, of each specimen, is 950 mm and both ends are embedded into steel tubes with grip length of 300 mm, L_a, using an anchor filler material - a 1:1 mixture by weight of epoxy resin and clean sand - along with 3D printed caps for alignment. Mechanical treatment - surface sanding - of specimen's ends before mounted into the anchorage is performed to promote adhesion of the rebar with the filler material [7,10,12,14,15].

A total of 39 specimens from 13 different rebar configurations are mechanically tested within this study. The sample size is statistically acceptable, as the low Coefficients of Variation (CoV) ensure the consistency of the obtained data. For both series of tests, the average value, standard deviation, and CoV for each property are calculated. Stress-strain curves are generated for each sample from the load and strain measurements recorded from the extensometer. The tensile strength and tensile modulus of elasticity are calculated according to the standard.

3.3.2 Fatigue tests

Tensile fatigue tests on three selected BFRP rebar designs are performed using Instron 500 Universal Testing Machine in accordance to B7_ACI 440.3R-04 standard [14]. All samples are tested under displacement control and a frequency of 1 Hz at room temperature. A sinusoidal loading pattern is used, and the load required to apply the target displacement is observed to decrease at each loading cycle during the test continually. A range of strain levels is selected in order to reach a number of cycles to failure ranging from 10^4 to 10^6. Throughout the whole duration of the fatigue cycling test, the applied load, displacement and specimen elongation are electronically recorded every 1000^{th} cycle.

3.3.3 Material analysis and evaluation using μ-CT

The internal microstructure of the manufactured braided BFRP composite rebars is examined using X-ray micro-computed tomography. More specifically, samples of 30 mm length are scanned using a Phoenix Nanotom M with DXR flat panel detector nanofocus CT system at the UCD Rosemount Environmental Research Station facilities. All scans are performed at a resolution of 4.2 μm over a 360° rotation using 2400 projections and 80 kV voltage. The total scan time is 2 hours and a stack of 1000 cross-sectional, greyscale digital images are produced. Image processing analysis is then performed using ImageJ & VG Studio Max software programs, and the main outcome is the detailed qualitative examination of composite samples. More specifically, the tomography is employed to fully evaluate the composite's geometrical properties. Geometrical consistency is validated including measurements on layer thickness, braiding angle and fibre orientation, size and shape of individual yarns (basalt and PET) along the yarn paths are measured, yarn cross-section deviations from the idealized elliptical shape and nesting effects are observed. Fibre volume fractions are calculated; defect development is carefully examined, and void content throughout the braid structure is accurately estimated; a 3D reconstruction model of each sample from μ-CT scanner datasets is finally completed. Detection of the composite's void area fraction and spatial distribution of enclosed voids are closely related to the overall quality of BFRP rebars. Voids are imperfections from the manufacturing process, causing anisotropy in the composite material and significantly affecting its mechanical properties. Composites with higher void content usually exhibit lower tensile strength and fatigue resistance. Microstructure analysis is necessary to assess both the quality and consistency of the braiding manufacturing process and improve the current braid geometrical models. Understanding the three-dimensional geometry of braided composites will lead to improved analytical models and realistic geometrical modelling towards simulation of their mechanical response with FEA methods [17,18].

4 RESULTS AND DISCUSSIONS

Selected results from this project are presented below. Table 3 exhibits the outputs of tensile tests on a fully braided and a hybrid (UN core) laboratory manufactured BFRP rebar. All properties are represented by average values with a sample size of 3. All specimens failed within the test section area, demonstrating a successful grip system [12].

Table 3. Test results for the two BFRP composite rebar designs.

Sample no	BFRP 1	BFRP 2
OD (mm)	8	
Fibre Volume Fraction (%) *	51.63	48.96
	Aver. / CoV	
Maximum Load (kN)	17.84/ 0.01	17.38/ 0.03
Ultimate Tensile Strength (MPa)	354.99/ 0.01	345.73/ 0.03
Maximum Displacement (mm)	10.09/ 0.05	10.50/ 0.06
Ultimate Strain (%)	2.59/ 0.06	2.50/ 0.10
Elastic Modulus (GPa)	14.76/ 0.02	14.27/ 0.06

* Note: Numerically calculated using CLT approach

Figure 2 shows the tensile stress-strain curves for all six specimens of the two different designs. The tested rebars show linear elastic stress-strain relationship up to failure and brittle fracture types, typical for all FRP products. When comparing the different design approaches, a similar mechanical behaviour is noticed; as the fibre volume fractions are increased from 48.96% to 57.76%, the elastic moduli also increase from 14.27% to 14.76%. Both samples exhibit a tensile strength comparable to the one of general steel bars (~ 400 MPa) and the maximum value - 355 MPa - obtained for the fully braided configuration. In addition, the tested specimens show a strain at failure ranging from 2.50% to 2.59% [12].

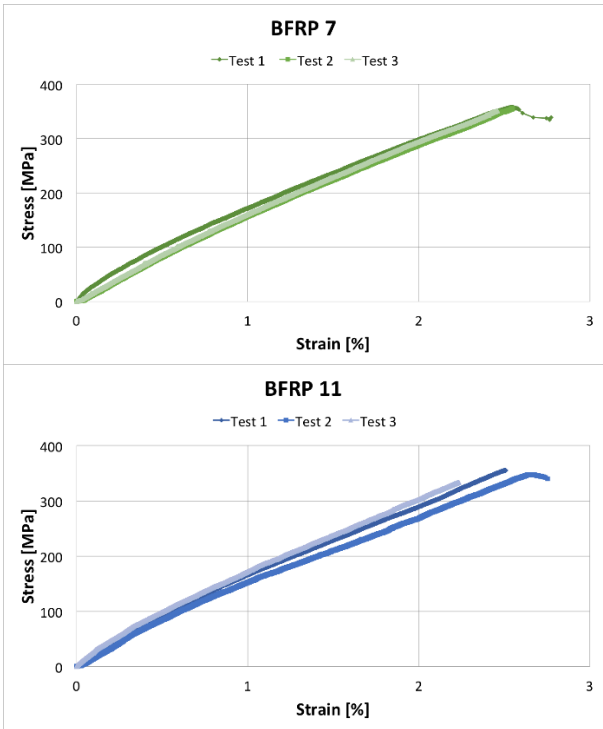

Figure 2. Stress – Strain curves for all manufactured BFRP rebars with an outer diameter of 8 mm

Tensile fatigue results confirm a sufficient fatigue performance of BFRP rebars. Samples with a lower fibre volume fraction and a higher void content seem to exhibit an increased fatigue stress sensitivity. It must also be noted that the dissipated energy method is used to evaluate the fatigue resistance of BFRP composites, as it takes into account the stiffness modulus of the material and its viscoelastic nature. Figure 3 illustrates μ-CT cross-sectional images from three different Z-axis locations - 0, 50, 100% of the sample's total length - that are segmented using an intensity threshold. Initial results show discrepancies on void area fraction within the sample, from 1.5 to 2.10% with an average void size of 0,040 mm^2.

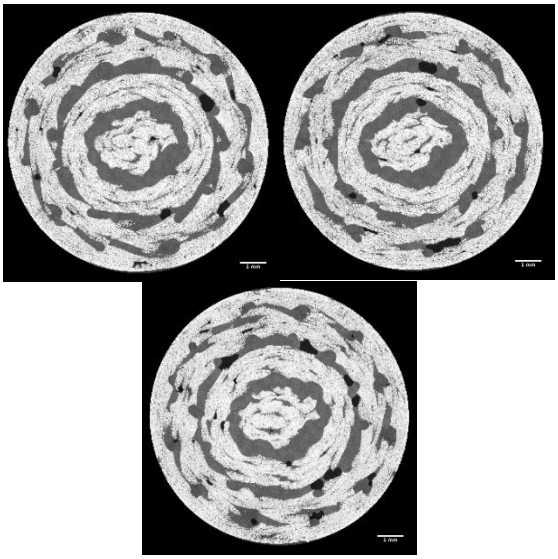

Figure 3. μ-CT cross-sectional images along the X-Y axis of sample BFRP 10

5 CONCLUSIONS

This chapter has reported on the research completed within TRUSS project regarding the development and characterisation of BFRP composite rebars using both braiding and hybrid designs. More specifically, the aim of this work has been to develop a better understanding of the mechanical behaviour of composite rebars and correlate it with the design and manufacturing process. An in-depth research on their strength, response, and durability has been the final objective of this project in order to obtain an optimized design and to determine how this promising material can contribute to a more durable infrastructure. The results have demonstrated a clear dependency of modulus and strength on both designing parameters (like internal architecture, number of layers, angle, yarn size, number of carriers) and fibre volume fraction. The mechanical response has been mainly dominated by the fibre architecture, which significantly affects localized properties, crack propagation and load redistribution in the material. The maximum tensile strength obtained, has been comparable to the one of steel and all design approaches have exhibited satisfactory mechanical behaviour. In general, the results obtained have contributed to a further understanding of the various available design approaches for BFRP composite rebars and their properties.

ACKNOWLEDGMENTS

This project has received funding from the European Union's Horizon 2020 research and innovation programme under the Marie Skłodowska-Curie grant agreement No. 642453.

REFERENCES

[1] Antonopoulou, S. and McNally, C. (2017), 'Reliability assessment of braided BFRP reinforcement for concrete structures', *Proceedings of 27th European Conference on Safety and Reliability (ESREL2017)*, Portorož, Slovenia.

[2] Benmokrane, B. and Ali, A.H. (2016), 'Durability of FRP rebars in aggressive environments', *Proceedings of 8th International Conference on Fibre-Reinforced Polymer (FRP) Composites in Civil Engineering (CICE2016)*, Hong Kong, China.

[3] Koch, G., Varney, J., Thompson, N., Moghissi, O., Gould, M. and Payer, J., *International Measures of Prevention, Application, and Economics of Corrosion Technologies Study*, NACE International Houston, Texas, USA: Gretchen Jacobson, 2016.

[4] Elgabbas, F., Ahmed, E.A. and Benmokrane, B. (2015), 'Physical and mechanical characteristics of new basalt-FRP bars for reinforcing concrete structures', *Construction and Building Materials*, 95, 623-635.

[5] Fiore, V., Scalici, T., Di Bella, G. and Valenza A. (2015). 'A review on basalt fibre and its composites', *Composites Part B: Engineering*, 74, 74-94.

[6] Hollaway, L.C. (2010), 'A review of the present and future utilisation of FRP composites in the civil infrastructure with reference to their important in-service properties', *Construction and Building Materials*, 24(12), 2419-2445.

[7] Antonopoulou, S., McNally, C. and Byrne, G. (2016), 'Development of braided basalt FRP rebars for reinforcement of concrete structures', *Proceedings of 8th International Conference on Fibre-Reinforced Polymer (FRP) Composites in Civil Engineering (CICE2016)*, Hong Kong, China.

[8] Portnov, G., Bakis, C.E., Lackey, E. and Kulakov, V. (2013), 'FRP Reinforcing bars - designs and methods of manufacture (Review of Patents)', *Mechanics of Composite Materials*, 49(4), 381-400.

[9] Birkefeld, K., Roder, M. and VonReden, T. (2012), 'Characterization of Biaxial and Triaxial Braids: Fiber Architecture and Mechanical Properties', *Applied Composite Materials*, 19, 259-273.

[10] Seo, D.W., Park, K.T., You, Y.J. and Lee, S.Y. (2016), 'Experimental Investigation for Tensile Performance of GFRP-Steel Hybridized Rebar', *Advances in Materials Science and Engineering,* 1-12.
[11] Ivey, M.A., Carey, J.P., and Ayranci, C. (2016), 'Manufacturing and Characterization of Braidtruded Fiber Reinforced Polymer Rebar', *Polymer Composites*, 39(2), 337-350.
[12] Antonopoulou, S., McNally, C. and Byrne, G. (2018), 'A comparative study on different BFRP rebar design methodologies', *Proceedings of the Civil Engineering Research in Ireland Conference (CERI 2018*), Dublin, Ireland.
[13] Bank, L. C., *Composites for construction: Structural design with FRP materials*, Hoboken, N.J.: John Wiley & Sons, 2006.
[14] ACI Committee 440, *Guide Test Methods for Fiber-Reinforced Polymers (FRPs) for Reinforcing or Strengthening Concrete Structures*, American Concrete Institute, ACI 440.3R-04, 2004.
[15] American Society for Testing and Materials, *Standard Test Methods for Tensile Properties of Fiber Reinforced Polymer Matrix Composite Bars*, Conshohocken, USA, ASTM D7205, 2011.
[16] Valentino, P., Furgiuele, F., Romano, M., Ehrlich, I. and Gebbeken, N. (2013), 'Mechanical characterization of basalt fibre reinforced plastic with different fabric reinforcements – Tensile tests and FE-calculations with representative volume elements (RVEs)', *Proceedings of Convegno Nazionale IGF XXII,* Italy, 231-240.
[17] Garcea, S.C., Wanga, Y. and Withers, P.J. (2018), 'X-ray computed tomography of polymer composites', *Composites Science and Technology*, 156, 305-319.
[18] Zeng, X., Endruweit, A., Brown, L. P. and Long, A.C. (2015), 'Numerical prediction of in-plane permeability for multilayer woven fabrics with manufacture-induced deformation', *Composites: Part A*, 77, 266–274.

Chapter 2: Reduction of uncertainty in assessing concrete strength in existing structures

Md Shah Nur Alam Sourav[1,2], Salam Al-Sabah[2], Ciaran McNally[1]
[1]Department of Civil Engineering, UCD, Belfield, Dublin, Ireland
[2]Arup, Dublin, Ireland
email: shah-nur-alam.sourav@ucdconnect.ie, Salam.Al-Sabah@arup.com, ciaran.mcnally@ucd.ie

ABSTRACT: This project proposes a new non-destructive method, known as Post-installed Screw Pull-out (PSP) test, with the aim of achieving reliability and accuracy in the assessment of compressive strength of concrete in actual structures. The method is partially destructive in nature. A standard concrete screw is installed in a hole that is drilled into the concrete, and the screw is subsequently pulled out of the concrete. In the PSP test, the loading arrangement ensures a complete pull-out failure where the failure occurs by the local crushing of the concrete underneath the threads of the screw. The peak load obtained during the pull-out is then correlated with the compressive strength of concrete. Extensive experimental study shows that the repeatability of the PSP test in terms of coefficient of variation is highly affected by the aggregate characteristics. The harder the aggregate particle in the concrete, the higher the coefficient of variation. The results show that the PSP test provides a higher degree of correlation with compressive strength in concrete with the softer aggregate particle, such as brick chips or lightweight aggregate, compared with the concrete having harder aggregate such as limestone. The study also includes the numerical investigation of the PSP test to investigate the failure mechanism involved. A commercial finite element program, Abaqus, is used to carry out the investigation and to perform the parametric studies.

KEY WORDS: Concrete strength; Non-destructive method; Repeatability; Strength relationship; Numerical simulation.

1 INTRODUCTION

Concrete is made of various combination of different constitutes, mainly cement, sand, aggregate and water. The final properties of concrete depend on the properties of its constituents, as well as its treatment in the construction site, e.g., its consolidation and curing procedures. Moreover, in real structures, concrete is accompanied by a significant amount of steel reinforcement, which induces more uncertainty to the overall properties. In many cases, the properties of concrete in the structures remains doubtful whether they have gained the desired values, or may be susceptible to degradation over the course of time that may affect the service life. Also, in many cases, due to lack of available information on concrete, the strength and performance of concrete in a structure remain uncertain. For these reasons, it is always necessary to assess the in-place properties of the concrete, either for quality assurance or for evaluation of the existing conditions. Non-destructive test (NDT) methods, either completely non-destructive or partially destructive, could be ideal as these methods do not impair the function of the structure and allow checking (not all NDTs though) of the properties at the same location to assess the change in properties in time [1]. Rebound hammer test, Ultrasonic Pulse Velocity (UPV) test, maturity test, and resonance frequency test are non-destructive while pullout test, Cut And Pull-Out (CAPO) test, pull off test, break off test, and penetration resistance test are partially destructive. All in-situ tests are generally termed as NDTs even though some of the test methods offer some superficial damage to concrete surface.

2 STATE OF THE ART

Core test is thought to be the most reliable method in the assessment of compressive strength of concrete in a structure [2]. Core testing in the practical field can be limited as the method is expensive, time consuming, technically difficult in some cases and even impossible in others. This led to the use of NDTs as an alternative of core testing when enough level of confidence is ensured by the established relationship of NDTs results with the core testing results. NDT methods are a useful approach with the benefits of low cost, fast application, portability and they sometimes provide the results instantly on site. NDT methods can offer a lower number of cores to be taken from the structures to allow the assessment of the concrete strength throughout the whole structure without deteriorating the quality of assessment [2-4].

Each of the test methods has its own limitations and applications [6]. Some methods cannot be directly applied to existing concrete without prior planning. Methods such as in-place pullout, in-place cylinder, stoll tork and maturity cannot be applied in old structures as they need the equipment to be cast in the fresh concrete. The resonance frequency method has never got out of the laboratory to be applied on site [7]. In the assessment of compressive strength of in-situ concrete, several points need to be considered:

- The ability of the NDT method to measure to the compressive strength,
- the variation of the measured NDT results,
- the variation of the material properties,
- the magnitude of the measurement error, and
- the use of correct statistical model.

The key feature of all NDT methods is that they all measure some properties other than compressive strength and relate the measured properties to the compressive strength empirically. NDTs those are totally non-destructive, such as rebound hammer or UPV, measure physical properties and their reliability in the assessment is found to be low. The best application of the totally non-destructive method are found to be uniformity checking and qualitative assessment of the concrete. Partially destructive methods measure some other strength properties, different from the compressive strength. They are found to have higher reliability in the assessment than totally non-destructive methods. The CAPO test is a method that arguably measures the property close to the compressive strength of concrete. The generalised relationship of CAPO test can predict the compressive strength with reasonable accuracy. The low cost, simplicity and the speed of the test dictates the popularity of the test methods. These factors contribute to the high popularity of rebound hammer and UPV to be used in laboratory and on site. The CAPO test, even though it is reliable enough to be used in practical field, has limited use in practice due to the high equipment cost.

The assessment quality of concrete strength is limited due to the sources of uncertainties arising at various levels and caused by the testing method itself, interference of the environment, material intrinsic variability, human error, and data interpretation. The interpretation of the NDT test results is a challenging task for the users of NDT methods. The validity of the relationships provided by the manufacturers of NDTs has often been questioned due to effect of factors acting on the NDT results. These factors cannot be quantified and often, are uncontrollable in practical field. As such, in most cases, the proposed relationships have been found to be providing inaccurate results when used for any other concrete. The general approach in the use of NDT results is to perform in-situ test and standard strength test at various strength levels and then to use the statistical procedures to establish the strength relationship. The uncertainty of the estimation of the concrete strength depends on the variability of the test results and the uncertainty of the obtained relationship.

The with-in variability or repeatability of the test method contributes to the uncertainty in the assessment. The within-test Coefficient of Variation (CoV) is about 3% for standard moulded specimens in the laboratory [8] and 5% for drilled cores [9]. The analysis of within-test variability can be an indicator of the precision of the method in the measurement of the compressive strength of concrete. Table 1 provides a general statement on the best use of the NDT methods, their repeatability in terms of coefficient of variation, and their accuracy in the strength prediction for normal weight concrete based on the literature. Only test methods, which can be directly applied to the in-situ concrete without any prior planning, are considered here. Repeatability (i.e., CoV) of the most test methods is in order of about 10%, whereas internal friction test has CoV of 15% indicating high variability in the test results. On the other hand, UPV test results show very low variability, though the strength prediction is severely affected by other factors.

Table 1. NDT methods: their best use, repeatability and probable accuracy in the strength prediction.

Test method	Best use	Repeat ability (CoV)	Strength prediction for 95% confidence limits
Rebound hammer	Assessing uniformity and quality	10% [3]	±30% on site [10]
UPV	Assessing uniformity and relative quality, severity of deterioration or cracking	2% [11]	±30-40% on site [5]
CAPO	In-situ compressive strength	8% [12]	±20% on site with general correlation [13]
Penetration Resistance	To assess the uniformity of concrete and to delineate zones of poor quality or deteriorated concrete	8% [14]	±20% (for specific aggregate) [15]
Pull off	To determine the tensile strength of concrete near to the surface, to determine the bond strength to the substrate or the tensile strength of either the overlay or substrate, whichever	10% [15]	±15% in the lab [15]
Break off	To determine the flexural strength of near surface concrete, not much use in recent years	9% [16]	±20% [13]
Internal friction	Not in use in recent years	15% [15]	±30% [13]
Friction transfer	Very limited use	10% [17]	---
Twist off	Very limited use	8% [18]	---

Based on an extensive literature review, a common statement that is applicable to most of the NDT methods is that whether used individually or in combination, none of the methods is capable of producing the true compressive strength value. The level of confidence in the assessment can only be improved by using the rational correlation established for the specific concrete. It is strongly argued in the research community that there is no unique set of relationship for NDT methods [5]. The coefficient of a particular mathematical model can vary over a large range. Again, the type of mathematical model for a particular set of concrete has little effect on the quality of fit in the practical field. This indicates that model error is smaller than error due to the measurement uncertainties [5]. Another important aspect to be investigated is the statistical validity of the established model.

The successful use of the NDTs in determining the in-situ strength of concrete relies on the degree of confidence obtained in the strength relationship for the concrete under investigation. Standards and guidelines are often available at national and international levels to better use the obtained results in an effective and meaningful way. The practical use of the NDT methods are currently dictated by cost, ease, and speed of NDTs, rather than the accuracy of the test results. Thus, NDT may not be able to serve the true purpose of its application. A better balance between the financial/technical advantages and

disadvantages of the NDT methods needs to be achieved for reducing the uncertainty of in-situ strength of concrete in practise.

3 PSP TEST: EXPERIMENTAL STUDY

3.1 Theoretical consideration

With the aim of obtaining an improved degree of accuracy at limited cost, a simplified test approach, labelled as "Post-installed Screw Pull-out" (PSP) test has been studied in the project [19-20]. The method is partially destructive in nature. A standard concrete screw is installed in a hole that is drilled into concrete. The screw is subsequently pulled out of the concrete. In the PSP test, the loading arrangement is such that a concrete cone failure does not occur, rather the failure occurs by complete pull-out of the screw involving crushing of the concrete present between the threads of the screw. The peak load obtained during the pullout is then correlated with the compressive strength of concrete.

A commercial pullout tester can be used for in-situ assessment. This offers a low cost method for carrying out the PSP test in comparison to core testing and some other available NDTs. The PSP test is quite easy to perform and simple as the test takes only 10-15 minutes. The damage in concrete associated with the test process due to the drilling of hole is minimal and has practically no effect on the structural capacity of the concrete members. An advantage of the test method is that the test provides a measurement of the direct interaction of the screw with the concrete.

3.2 Push-in test mechanism

In a preliminary investigation and also due to the lack of available facilities in the laboratory, a push-in mechanism was tried. Threads of the screw interact similarly as PSP test when a screw is pushed inside a concrete [21]. A void underneath the screw is placed to facilitate the movement of the screw. Movement of the screw is associated with the crushing of concrete under the threads. The mechanism is similar to the mechanism observed during the complete pullout failure that occurs during PSP test. An investigation with mortar shows a high correlation of the push-in load with the compression strength (Figure 1).

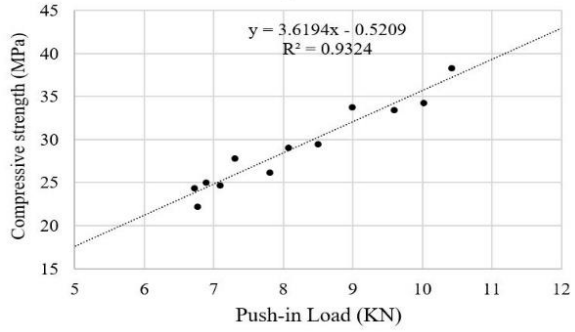

Figure 1. Strength relationship of Push-in test mechanism in mortar.

3.3 PSP test: Load-displacement curve

The PSP test measures the peak load during the pullout of the screw from the concrete sample following the complete pullout failure in the concrete. The typical load displacement curve for a PSP test (Figure 2) shows that almost all curves follow a similar pattern in which stiffness varies from strong to weak, with the initial stiffness being almost linear. The peak load occurs following the softening behaviour of the curve. This peak load indicates the maximum resistance of the material between the threads against the pullout force. The curve then follows a negative slope and the shearing of the remaining portion of materials under the threads along the outer edge of the screw threads continues forming a shear band. A complete shearing surface is formed along the outer edge of the threads as the screw moves a distance nearly equals to the pitch of the threads. Following this stage, the remaining acting force resisting the movement of the screw is a result of the possible small mechanical interlock between the threads and the damaged materials, and friction. These forces remain almost constant for the following screw movement.

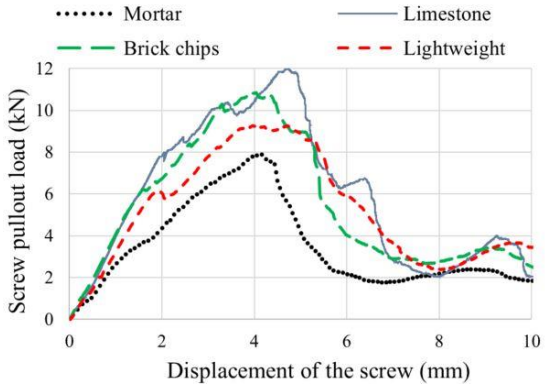

Figure 2. Typical load-displacement curve in PSP test

3.4 PSP test: Repeatability

Figure 3 shows the with-in test repeatability in terms of CoV of PSP test as percentage as a function of average screw pullout load. This figure illustrates the degree of scatter in the PSP test results. Mortar and concrete having lightweight and brick chips aggregate resulted in lower values (mean values are around 7%, 9% and 9% respectively) in comparison to concrete with limestone (mean value of around 16%), depicting the higher consistency of the PSP test in mortar and concrete with softer aggregate. Concrete with limestone aggregate shows higher variability attributing the pronounced influence of the harder aggregate on the PSP test.

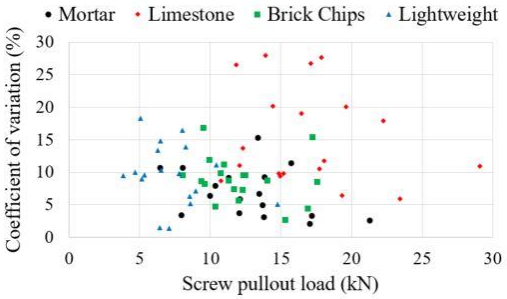

Figure 3. With-in test repeatability of PSP test.

3.5 PSP test: Effect of aggregate type

The results of PSP test and corresponding compressive strength are presented in Figure 4, showing that there is a clear trend of increase in pullout load of PSP test with the increase of compressive strength of concrete. The effect of aggregate type

on the PSP test can be clearly demonstrated from Figure 3 (showing the repeatability of the test) and Figure 4. Different types of aggregate lead to different peak loads depending on the elastic modulus and strength of aggregates used in concrete. Concretes containing limestone aggregates shows higher screw pullout load than mortar and the concretes of similar compressive strength containing brick chips and lightweight aggregates.

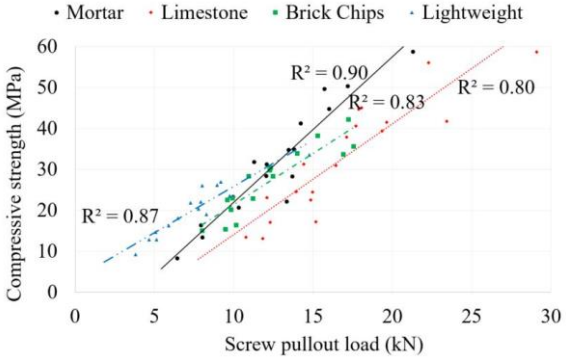

Figure 4. Strength relationship of PSP test.

3.6 PSP test: Strength relationship

Figure 4 shows the simple best-fit linear relationships between the compressive strength and screw pullout load for mortar and concrete. Good correlations are observed for mortar and concrete with lightweight aggregate having an R-squared value of 0.90 and 0.87 respectively. Concrete with limestone and brick chip aggregate result in R-squared values of 0.80 and 0.83 respectively. All the relationships follow a similar slope, except that of mortar. When all the datasets are combined, an R-squared value of 0.73 is obtained. An R-squared value of 0.75 is found with the datasets of all concrete only, except the mortar. Mean residual as a measure of error is around 5 MPa for the concrete with limestone whereas mortar and concrete with other aggregates result in mean residuals of around 3 MPa.

4 PSP TEST: NUMERICAL STUDY

A numerical investigation of the PSP test is carried out to investigate the failure mechanism involved. A commercial finite element program, Abaqus, is employed for this purpose.

4.1 Material modelling

A Concrete Damaged Plasticity (CDP) model defined in Abaqus [22] is used for modelling concrete material. The plastic-damage model in Abaqus is based on the models proposed by Lubliner et al [23] and by Lee and Fenves [24], which allows for two main failure mechanisms of the concrete material, tensile cracking and compressive crushing. Concrete strength of 40 MPa is considered. The related material input such as elastic modulus, and the complete stress-strain curve for compression are derived using the fib Model Code 2010 [25]. Density and Poisson's ratio are taken to be 2400 kg/m^3 and 0.18 respectively. The dilation angle is assumed to be 35^0, the shape factor $k_c = 0.667$, the stress ratio $f_{b0}/f_{c0} = 1.16$, and the eccentricity = 0.10.

Figure 5 shows the stress-strain in compression to be used for the input in Abaqus. In tension, the maximum tensile stress and fracture energy are used to reduce the effect of mesh density on the results. Corresponding damage parameters for compression and tension are introduced in both tension (Figure 6) and compression (Figure 7) respectively. Damage in concrete is considered to occur in the softening branch in both tension and compression. Screw is modelled as purely elastic steel material as no screw failed during the experimental investigation and the interest in the stress distribution in steel is neglected as such.

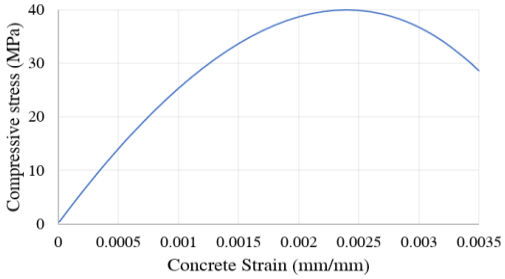

Figure 5. Concrete Stress-strain curve in compression.

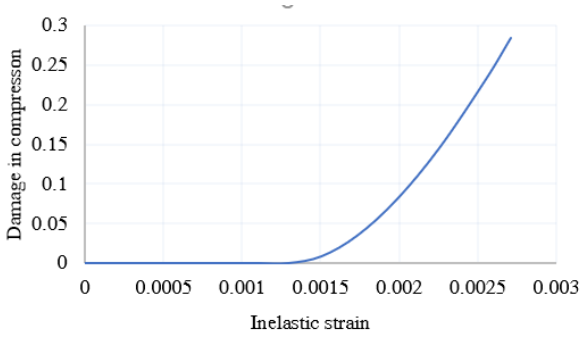

Figure 6. Compressive damage-inelastic strain relationship.

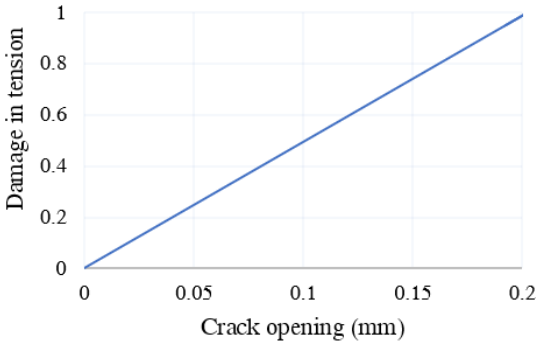

Figure 7. Tensile damage-crack opening relationship.

4.2 Numerical methods

A challenging task in the numerical study is to model the progressive failure in concrete using the CDP model in Abaqus. The model does not support the element deletion in Abaqus/CAE interface and thus using the Lagrangian mesh results in severe distortion of the mesh, which ultimately results in the non-convergence of the simulation. Introduction of element deletion can resolve some of the issues related to the excessive distortion of the elements, but it also introduces new issues involving conservation of mass. A meshless technique such as Smooth Particle Hydrodynamics (SPH) can provide the formulation of progressive failure in the material. Use of connector element is found in literature to define the behaviour of the steel rebar-concrete interaction [25-26]. Adaptivity technique to improve the mesh quality and remesh during the progress of the analysis can help to get a converged solution.

Arbitrary Lagrangian Eulerian (ALE) adaptive meshing can be used in conjunction with traditional Lagrangian mesh where severe distortion of the mesh occurs [22].

4.2.1 Traditional Lagrangian mesh

An axisymmetric model is used in this case. The interaction between the screw and concrete is modelled using the contact interaction. Surface to surface interaction with frictionless contact is used in the tangential direction and hard contact property is chosen along the normal direction. Figure 8 shows the damage due to compression in the concrete for 7.3 mm displacement (though 8 mm displacement was applied in the model) of the screw. The model shows a complete damage of the material due to compression starting from the bottom of the thread extending towards the reaction ring. Tensile damage in the concrete is shown in Figure 9 where a noticeable tangential cracking can be observed near the bottom threads of the screw. During the experimental investigation of the PSP test, these types of compression crushing and tensile cracking are not observed.

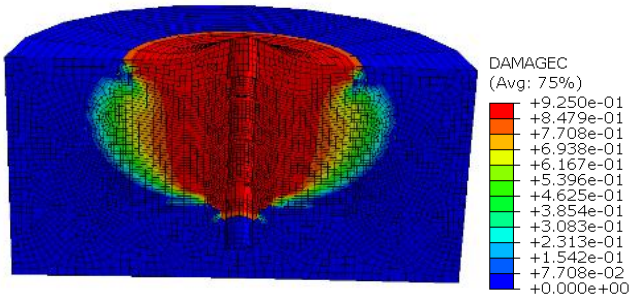

Figure 8. Compressive damage in concrete in Lagrangian mesh.

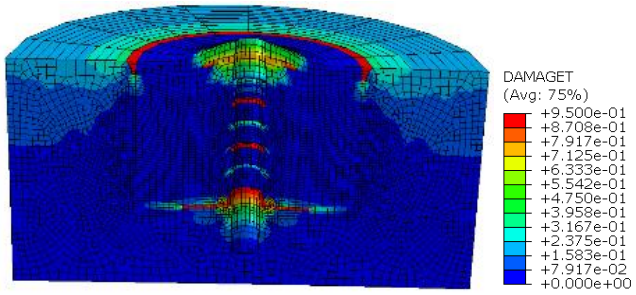

Figure 9. Tensile damage in concrete in Lagrangian mesh.

4.2.2 SPH method

SPH is a numerical method that is part of the larger family of meshless (or mesh-free) methods. For these methods, there is no need to define nodes and elements; instead, only a collection of points are necessary to represent a given body. SPH analyses are effective for applications involving extreme deformation. Abaqus offers a method to convert Lagrangian finite elements to SPH particles based on the chosen criteria, such as time, stress, and strain. Converting to SPH particles offers an improvement over the element deletion option because the generated particles are able to provide resistance to deformation beyond finite element distortion levels [21].

In the SPH model, the portion of the concrete present in between the threads and extending up to the reaction ring is modelled due to limited capacity of the computing machine and also to reduce the computational time. Figure 10 shows the arrangement of the screw and the concrete used in the simulation. A strain based criteria (maximum principle strain = 0.2) is chosen to convert the Lagrangian element into SPH particle.

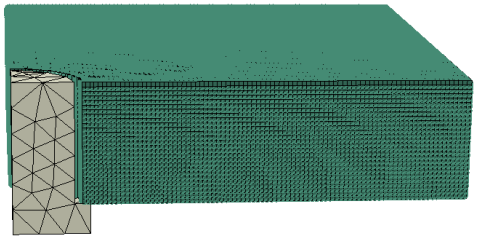

Figure 10. SPH model of the PSP test.

4.2.3 Connector elements

A 1/4 of a 3D model is formulated here to reduce the computational time. Slot and align type connectors are used in conjunction to simulate the transfer of forces from the screw to the concrete. These special elements connect the nodes at the interface between the concrete and screw in the longitudinal (pullout) direction. In total 48 connectors are used along the length of the screw and around the circumference (Figure 11). The connector behavior is defined as a spring with a non-linear elastic behavior obtained from the force-displacement relationship of a particular set of similar grade concrete as defined in the material model. Figure 12 shows the force-displacement relationship. A hard contact is employed in the other directions.

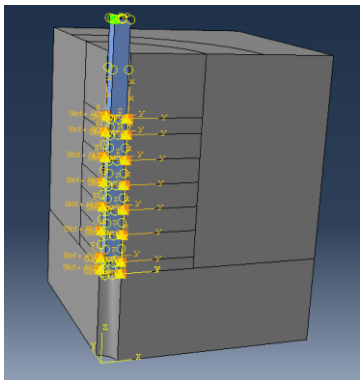

Figure 11. Connector elements to represent the interaction between screw and concrete.

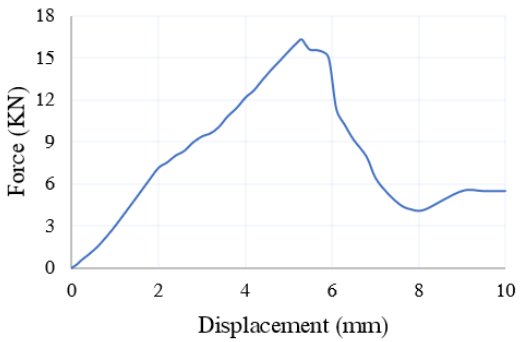

Figure 12. Force-displacement curve in a PSP test.

Damage due to compressive and tensile failure occurring in concrete during the PSP test are shown in Figures 13 and 14

respectively. These two figures also confirm that damage due to compressive crushing and tensile cracking occurs only around the threads of the screw, as is the case in the PSP test.

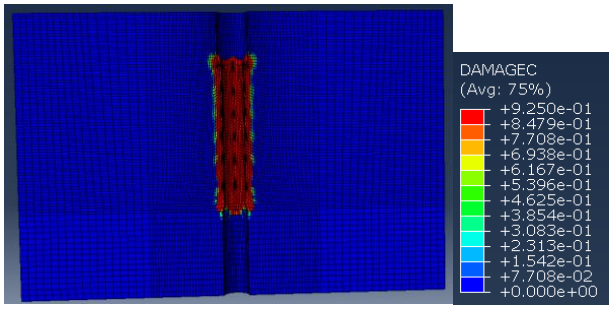

Figure 13. Damage in the concrete due to compression.

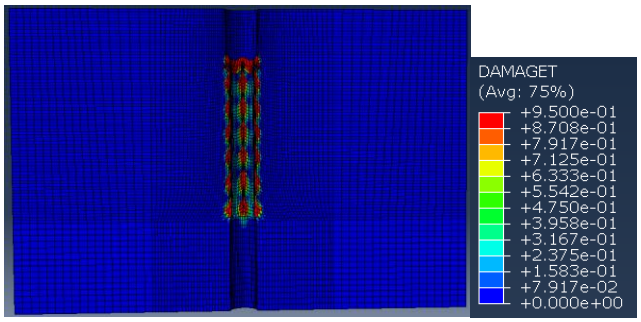

Figure 14. Damage in the concrete due to tension.

5 CONCLUSIONS

A PSP test has been developed to improve the reliability of strength assessment in a cost-effective way. Experimental studies on the PSP test have shown the potential to be reliable and reasonably accurate, especially in concrete with soft aggregate, such as brick chips, and lightweight aggregate, yet cost effective compared to core testing and some other NDTs. This will ultimately contribute to the reduction of the uncertainty in the compressive strength assessment of concrete in existing structures. A conclusive methodology to describe the failure mechanism of concrete in the PSP test using numerical investigations is in progress, and a direct application of the test on site is planned for a later phase of the investigation.

ACKNOWLEDGMENTS

This project has received funding from the European Union's Horizon 2020 research and innovation programme under the Marie Skłodowska-Curie grant agreement No. 642453.

REFERENCES

[1] N.J. Carino, *Nondestructive test methods,* in *Concrete construction engineering handbook*, 2nd ed., Edward G. Nawy, Ed. Boca Raton, USA: CRC press, 2008.

[2] J. H., Bungey, S.G. Millard and M.G. Grantham, *Cores*, in *Testing of concrete in structures*, 4th ed., London & New York: Taylor & Francis, 2006.

[3] ACI Committee Report 228.1R, *In-Place methods to estimate concrete strength*, 2003.

[4] A. C. 437 and A. C. 437, *Strength evaluation of existing concrete buildings*, ACI 437R-03, Concrete Repair Manual, 1-28, 2003.

[5] Breysse, D. (2012), 'Nondestructive evaluation of concrete strength: An historical review and a new perspective by combining NDT methods', *Construction and Building Materials*, 33, 139-163.

[6] Sourav, M.S.N.A., Al-Sabah, S., and McNally, C. (2016), 'Strength assessment of in-situ concrete for the evaluation of structural capacity : State of the art', *Proceedings of Civil Engineering Research in Ireland Conference (CERI 2016)*, Galway, Ireland.

[7] Malhotra, V.M. and Sivasundaram, V. *Resonant frequency methods*, in *Handbook on Non Destructive testing of concrete*, 2nd ed., Boca Raton, USA: CRC press, 2004.

[8] ASTMC39/C39M-03, *Standard test method for compressive strength of cylindrical concrete specimens*, 2003.

[9] ASTM C 42/C 42M-03, *Standard test method for obtaining and testing drilled cores and sawed beams of concrete*, 2003.

[10] Malhotra, V.M., *Surface hardness method*, in *Handbook on non destructive testing of concrete*, 2nd ed., Malhotra, V. M. and Carino, J. N. Eds. Boca Raton, USA: CRC Press, 2004.

[11] ASTM C597, *Standard test method for pulse velocity through concrete*, 2009.

[12] ASTM C 900 - 15, *Standard test method for pullout strength of hardened concrete*, 2015.

[13] Bungey, J. H, Millard, S. G., and Grantham, M. G. *Partially destructive strength tests*, in *Testing of concrete in structures*, 4th ed., Abingdon, England: Taylor & Francis, 2006, 82-119.

[14] ASTM C 803/C 803M-03, *Standard test method for penetration resistance of Hardened Concrete*, American Society for Testing and Materials, 5-9, 1991.

[15] BS 1881-207:1992, *Testing concrete. Recommendations for the assessment of concrete strength by near-to-surface tests*, 1992.

[16] Johansen, R. (1979), 'In Situ strength evaluation of concrete: The Break-off method,' *Concrete International*, 1(9), 45-51.

[17] Naderi, M. (2005), 'Friction-transfer test for the assessment of in situ strength and adhesion of cementitious materials,' *Construction and Building Materials*, 19(6), 454–459.

[18] Naderi, M. (2006), 'Assessing the in situ strength of concrete , using new twist-off method,' *International Journal of Civil Engineering*, 4(2), 146-155.

[19] Sourav, M.S.N.A., Al-Sabah, S., and McNally, C. (2018), 'Use of post-installed screws in the compressive strength assessment of in-situ concrete', *Proceedings of the 6th International Symposium on Life-Cycle Civil Engineering (IALCCE 2018)*, Ghent, Belgium.

[20] Sourav, M.S.N.A., Al-Sabah, S., and McNally, C. (2018), 'Statistical reliability of the screw pullout test in the assessment of in-situ concrete strength', *Proceedings of Civil Engineering Research in Ireland Conference (CERI 2018)*, Dublin, Ireland.

[21] Sourav, M. S. N. A., Al-Sabah, S., and McNally, C. (2017), 'Post-installed screws for in-situ assessment of mortar strength,', *Proceedings of the 27th European Safety and Reliability Conference (ESREL 2017#0*, Portorož, Slovenia.

[22] Abaqus 2016 Documentation. [Online]. Available: http://130.149.89.49:2080/v2016/index.html. [Accessed: 22-Oct-2018].

[23] Lubliner, J., Oliver, J., Oller, S., and Oñate, E. (1989), 'A plastic-damage model for concrete', *International Journal of Solids and Structures*, 25(3), 299–326.

[24] Lee, J. and Fenves, G. L. (1998), 'Plastic-Damage model for cyclic loading of concrete structures', *Journal of Engineering Mechanics*, 124(8), 892–900.

[25] CEB-FIP Report, *Bond of reinforcement in concrete: State of the art*, FIB Bulletin 10, no. December, p. 434, 2000.

[26] Du, Q. (2015), *Finite element modelling of steel/concrete bond for corroded reinforcement*, Department of Civil Engineering, University of Ottawa, Canada: Doctoral thesis.

Chapter 3: Reduction of uncertainty in design of free standing nuclear spent fuel racks

Alberto González Merino[1,2], Luis Costas[2], Arturo González[2]
[1] Department of analysis and design, Equipos Nucleares, Avda. Juan Carlos I, 8 Maliaño, 39600, Spain
[2] School of Civil Engineering, University College Belfield, Dublin 4, Ireland
email: alberto.gonzalezmerino@ucdconnect.ie, costas@ensa.es, arturo.gonzalez@ucd.ie

ABSTRACT: The storage of nuclear-spent fuel generated during the operation of a nuclear reactor is considered a troubling safety issue. The recent accident at the Fukushima Daiichi Nuclear Power plant highlights the importance of a safe seismic design. The number of stored fuel assemblies has considerably increased during the last years due to the suspension of the fuel reprocessing. As part of ENSA activities in the nuclear power market, the design and manufacture of spent fuel storage racks is encompassed. Their seismic response governs the structural design as well as their layout within the spent fuel pool.

This project applies reliability methods with stochastic variables to perform a forward uncertainty propagation through the rack seismic analysis and assess the level of uncertainty currently existing in the most relevant outcomes. The uncertainty analysis investigates the variation in the outputs as a consequence of a variation in the input variables. Hence, the variables with a meaningful impact on the rack seismic response are identified and sampled, numerical simulations are conducted, transient results are filtered, and finally, key quantitative outputs are obtained. Then, theoretical statistical distributions are inferred, response surfaces are mathematically approached, Sobol indices are computed from variance-based sensitivity analysis and a reliability analysis is finally carried out to compute the probability of failure and to find out the design point. All of this provides insight about the rack seismic response and useful advises and rule of thumbs for future designs. In parallel, experimental vibration tests validate the current analysis methodology and its assumptions. The unavoidable scatter between experimental and numerical simulations is considered acceptable as numerical outputs show a good agreement in terms of order of magnitude with the experimental data.

KEY WORDS: Fuel storage racks; Seismic analysis; Uncertainty.

1 SPENT NUCLEAR FUEL STORAGE

The desire to meet the requirements of an increasingly energy-hungry world without the carbon emissions associated with fossil-fuel-fired power plants brings nuclear energy back into consideration. According to the World Nuclear Association, 502 additional nuclear reactors are expected to be operational by 2030. However, after the accident at the Fukushima Daiichi Nuclear Power Plant, concerns over the nuclear safety have greatly increased. Such an accident demands revaluations of the seismic margin and risk assessments. In particular, special attention is paid to the spent fuel storage facilities. Most pools were built to accommodate 1 1/3 core of spent fuel, but their number of stored fuel elements has considerably increased during the last years due to the suspension of the fuel reprocessing. The nuclear regulatory authorities classify them as seismic Category I structures which are required to remain functional during operation bases and safe shutdown earthquake conditions.

Depending on the nuclear reactor design, removal of a quarter to a third of the nuclear fuel elements in the reactor is approximately every 12 to 24 months. The spent fuel elements are temporary kept in wet storage pools until they are sufficiently cooled to permit them to be transferred to an alternative dry storage site. Fuel was originally stored in metallic racks with large centre-to-centre spacing to ensure subcriticality. These early-stage rack units were anchored to the pool embedments and braced to the pool walls. However, as the lifecycle of the reactor is prolonged, the fuel reprocessing is suspended, and the permanent storage repositories are delayed, plant owners have been storing all of their spent fuel on site. In order to accommodate the increasing inventory of fuel, the traditional racks have been progressively replaced by high-density fuel racks. In this new rack design, the storage capacity is maximized thanks to the use of neutron-absorbing materials that maintain subcriticality even for a reduced pitch spans. However, this extra fuel mass leads to additional inertial loads which boost the structural stresses during an earthquake event. To reduce these seismic loads the modern ‘freestanding’ design (just resting on the pool floor) is promoted. The rack bases are isolated from the pool floor and energy is dissipated through frictional hysteresis. Moreover, this design is oriented to facilitate the rack installation in such a radioactive environment with difficult access, making the installation as easy and quick as possible with no fixation to the pool.

2 INTRODUCTION TO FREE-STANDING RACKS

Spent fuel storage racks are used in the first step of the nuclear waste management process, during the wet storage of the irradiated fuel assemblies removed from the nuclear power reactor. Racks are metallic structures equipped with an array of rectangular parallelepiped storage cells forming a vertical cubbyhole supported by a rigid pedestal, as illustrated by Figure 1. Rack units are 5 m tall steel structures and can weigh up to 60 tons when fully loaded.

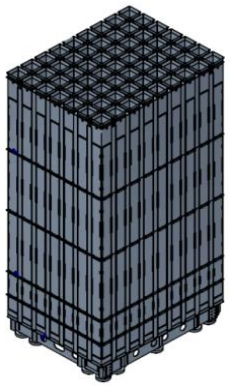

Figure 1. Sketch of a rack unit.

The number of cells depends on the size of the rack unit and the residual radioactivity of the spent fuel. Each cell is designed to store a single fuel assembly. Their dimensions depend on the type of reactor. Fuel assemblies are vertically threaded from the top, leaving relatively large gaps (5 to 12 mm) between the fuel element and the storage cell to ensure a smooth penetration and to avoid any damage in the assemblies. Differences in design and fabrication details can result in significant differences in the stiffness and natural frequencies of the rack modules.

Several independent rack units compose the storage system. The geometric dimensions and slenderness ratio of the racks are customized to fit within the existing pool. Clearance spaces between units are reduced as much as possible to maximize the storage capacity of the pool. Gaps between adjacent rack modules range between zero and 50 mm, while clearances between the peripheral modules and the pool walls are generally larger, ranging from 50 to 300 mm.

Rack units rest in the depths of the spent fuel submerged under a 12 m water head, to keep the fuel cool while providing an effective neutron shielding. Their free-standing conditions isolate their bases from the pool floor to reduce structural stresses during an earthquake. However, such a singular design complicates their seismic analysis involving complex physical phenomena such as rigid body sliding and tilting motions, frictional effects, support uplifts and impacts, collisions between adjacent units, fuel rattling, fluid-structure interactions, etc. Hence, an accurate estimation of the rack seismic response regarding their sliding displacements and reactions on supports is essential to achieve a safe pool layout and a reliable structural design.

3 SEISMIC ANALYSIS METHODOLOGY

Several approaches have been used to date in order to overcome the aforementioned challenges. However, an ad-hoc analysis methodology developed in the 80s is still applied nowadays with minor enhancements [1-10]. Such an analysis methodology carries out an implicit integration of the equation of motion across the earthquake duration. The methodology implements the hydrodynamic mass concept on a structural Finite Element (FE) analysis. Dynamic contact elements with gap capability are used to resemble the geometrical nonlinearities associated with the large displacements. The hydrodynamic mass concept modifies the mass matrix to simulate the hydrodynamic forces of the water action. Implicit integration algorithms solve the equation of motion at multiple time steps to simulate the transient response of the rack units. However, some dispersion of results still remains as numerical outputs greatly fluctuate as a consequence of the assumed input data, modelling procedures, and integration controls. This uncertainty in the deterministic analysis has traditionally been counterbalanced with conservative safety factors following guidelines based on practice. However, questions are raised with regard to the levels of uncertainty and the ranges of validity of the analytical results.

4 UNCERTAINTY OF THE SEISMIC ANALYSIS

Sliding displacements determine the potential collisions between units and pool walls, and impact forces on the supports represent the design loads for the rack feet and pool floor during a seismic event. The United States Nuclear Regulatory Commission has issued overall design requirements and licensing acceptance criteria for the performance of racks [11-13]. However, the rack seismic response is highly sensitive to a number of variables and therefore difficult to predict. The uncertainties associated with stochastic input variables (geometry, loads, excitation, friction, damping, etc.), the inherent assumptions, the modelling approach, the analysis controls and the vendors' judgements in the definition of the bounding load cases, contribute to the overall output uncertainty and cause dispersion on the numerical results.

The level of uncertainty, together with the significant loads and the critical issues involved, have been a source of concern to the nuclear regulatory authorities. The complexity of the analysis raises questions regarding the uncertainty propagation and the range of validity of the computations. Real safety margins are extremely difficult to predict in such a nonlinear system, so further uncertainty quantifications are requested as part of the approval and licensing process. As shown by Figure 2, the uncertainty range for best estimate calculation should always remain under the acceptance criterion.

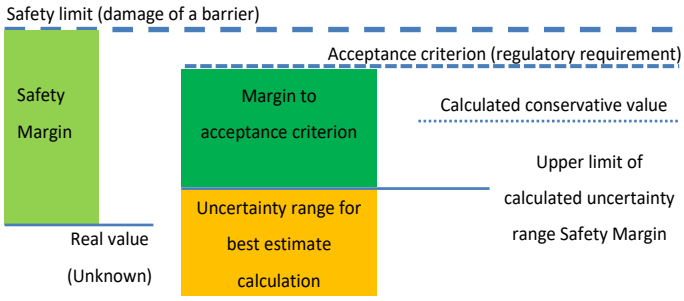

Figure 2. Concept of safety margins.

5 OUTLINE OF THE RESEARCH

This research provides an approach for uncertainty quantification in the rack seismic analysis based on probabilistic methodologies. A number of uncertain input variables are assumed to induce probability distributions in the output space. The implementation of this approach includes sampling techniques, surrogate modelling and reliability methods for uncertainty quantification. Figure 3 shows the global framework used in this uncertainty quantification.

5.1 Analysis methodology

In a first stage (Step A in Figure 3), the state of the art of the rack seismic design is summarized. The current analysis

methodology is introduced, and the different FE models are described. From the auxiliary models to the seismic analysis itself, the implicit conservatism and inherent simplifying assumptions are identified and discussed. Potential weakness restricting the range of applicability of the current analysis methodology are pointed out. Moreover, the algorithms for implicit integration of the nonlinear equation of motion are reviewed, and the application of the hydrodynamic mass concept is investigated.

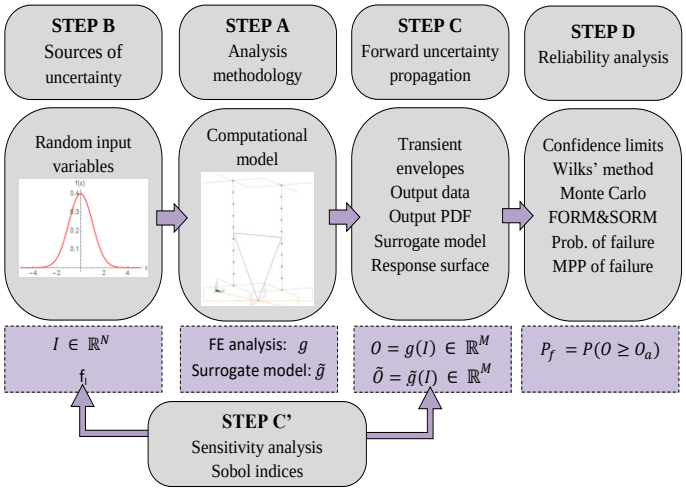

Figure 3. Global framework for uncertainty quantification.

This analysis methodology is subsequently verified and validated through comparison of the numerical simulations with experimental results collected from vibration tests. The outputs of the transient nonlinear analysis are therefore considered representative of the rack response.

5.2 *Sources of uncertainty*

In a second stage (Step B in Figure 3), the sources of uncertainty existing in the analysis methodology are identified and investigated. The variables with potential influence on the numerical simulations of the rack seismic response are listed by groups: load data, modelling properties, and solution controls. The stochastic input variables, the suitability of the conceptual FE model, the influence of modelling properties describing the physical behaviour and the accuracy of the user-defined integration controls are examined. The influence of the type of finite elements, the nodalization, the definition of the seismic load (i.e., as a force, displacement or acceleration time-history), the numerical algorithm, the type of solver, the Newton-Raphson features, etc., on the displacement and force response of rack are subjected to investigation.

The rack response is therefore assumed to entirely depend on the distributions of these input variables. Then, a validation, verification and calibration process is encompassed for the problem at hand. Preliminary one-factor-at-a-time parametric analyses are carried out. This technique examines the impact on the main transient outputs when one parameter is varied, and the others remain at their nominal values. Numerical results provide the first source of insight into the general behaviour of the rack system around their nominal values. They show a highly sensitive response with no asymptotic behaviour.

5.3 *Forward uncertainty propagation*

In a third stage (Step C in Figure 3), a forward uncertainty propagation, as in Figure 4, is carried out. Uncertain variables such as friction coefficients, contact stiffnesses, damping ratios, integration algorithm, convergence tolerances, etc., are difficult to estimate or measure. Therefore, wide uniform distributions are preliminarily specified to take into account random uncertainties associated with these variables. Sample sets are randomly generated via the Latin Hypercube Sampling (LHS) for the Design of Experiments (DoE) in order to effectively explore the multidimensional input space. Multiple deterministic simulations are conducted in ANSYS Mechanical using in-house macros to automatize the analysis process. These scripts update the model with the new set of input variables, launch the analysis and export the results via the command console. These numerical simulations return the transient response for the given sets of input variables. The outputs of main interest to the rack design are analysed from a probabilistic point of view. Transient envelopes of response are computed for the maximum sliding displacement and maximum force on supports. A quantitative approach to their respective bounds is conducted independently of the instant they occur. Probability Density Functions (PDFs) are inferred, and output statistics are provided. The Coefficient of Variation (CoV) quantifies the total uncertainty propagation for each output.

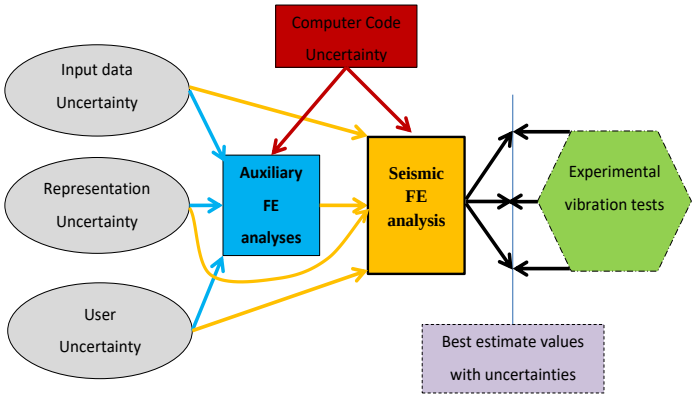

Figure 4. Flow diagram of the uncertainty propagation in the rack seismic analysis.

The propagation of uncertainties plays a dominant role in the transient analysis since the outputs at the end of a time step in the integration process are taken as initial conditions for the following step of the calculations. The uncertainty cumulated over all these stages may affect the final outputs in an expansive manner. This uncertainty analysis sets the boundaries of the transient response, provides the multivariate sensitivities and identifies the governing variables where additional testing is needed. It also provides an insight into the combined influence of input variables.

Furthermore, surrogate models based upon the Polynomial Chaos Expansions (PCE) are developed as cost-effective black boxes to emulate the numerical simulations. Surrogate models represent synthetic approximations to the response surface and have fundamental significance in the understanding of the rack design problem. Their analytical equations make possible to carry out multivariate sensitivity analyses with Sobol indices.

Such a sensitivity analysis highlights the influence of the inputs variation in the rack response. The influence of each input variable is quantified by groups: modelling process, user-defined analysis parameters, and stochastic input data.

5.4 *Reliability methods*

In a fourth stage (Step D in Figure 3), confidence intervals are calculated from the output distributions through the direct application of the Wilks' formula and statistical inference. The former sets the minimum number of simulations required to provide tolerance limits with a certain confidence level for a given probability content. The latter refines these tolerance limits by assuming a theoretical output distribution. Moreover, response surfaces of the racks seismic response are assessed from 500 deterministic simulations for the main 17 input variables. Surrogate models are built using 2nd order PCEs to emulate the rack response with reasonable accuracy.

Finally, different reliability methods are applied through the surrogate models. Monte Carlo simulations compute the probability of failure for both maximum sliding displacements and maximal forces on support. In addition, approximation methods find out the Most Probable Point (MPP) of failure and provide the coordinates of the MPP in the Hasofer-Lind standardized input space. The coordinates represent the values of the input variables leading to both types of failures. The associated director cosines highlight which variables push for the given type of failure.

5.5 *Experimental vibration tests*

In parallel, experimental vibration tests are conducted on a unidirectional shaking table. The testing campaign is carried out through a Spanish collaboration between Instituto de Hidraúlica de Cantabria and Equipos Nucleares S.A. in Spain. This collaboration aims to enlarge the knowledge acquired from previous experimental studies on isolated racks [14-19], by focusing on the interaction between more than one unit. For that purpose, a functional scaled 2-racks model is tested on a unidirectional vibration table for different initial configurations.

Both units are equipped with fake fuel assemblies, submerged in free-standing conditions inside a rigid steel pool and allowed to move on their own. This innovative multi-rack configuration is considered a world-premiere experience that allows the observation of the interactions between units for the first time. A hydraulic jack excites the physical model with a given acceleration time-history. A set of sensors and gauges monitor the transient response of the system. Accelerometers track the acceleration of the pool and units. Load cells measure the impact forces on the rack supports as well as the fluid forces at the centre of the rack faces. Video cameras record the transient displacements and rotations.

Figure 5 shows the sliding displacements of the two racks over the pool floor. Clearly, the two rack units move nearly in phase and with similar amplitudes. As accelerations are applied to the system, the racks separate from each other until reaching a gap of 8 mm at the end of the earthquake. Finally, the collected data are compared with the numerical outputs showing a good agreement in results exhibiting the same order of magnitude. There is evidence of a water-coupling effect leading to an in-phase motion of the units. The low water velocities and small relative deflections endorse the assumption of potential water flow. Hence, the analysis methodology is validated.

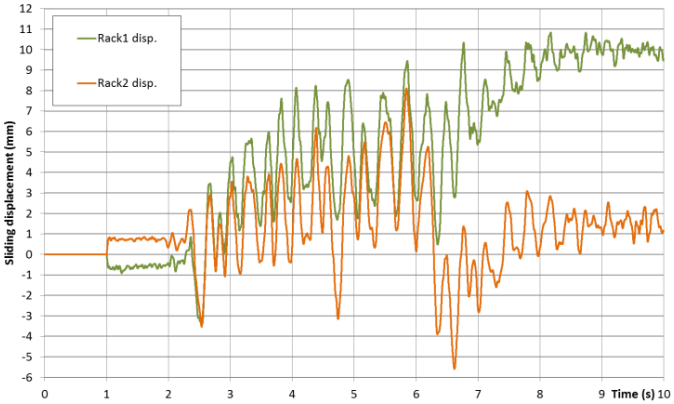

Figure 5. Sliding displacements of the two rack units.

6 CONCLUSIONS

Nuclear power plants are responsible for the management of the spent fuel removed from their reactor. The latter generally consists of using closely spaced racks submerged in a pool to store and cool the nuclear fuel. The modern free-standing design isolates the rack base from the pool floor and therefore reduces the seismic loads. However, their seismic response is difficult to predict accurately since it deals with transient inertial forces, geometrical nonlinearities, and fluid-structure interactions. Rack units may, therefore, slide over the pool liner while rocking, turning and twisting. The boundaries of these motions are provided by physical contacts that show up between racks and pool, fuel and racks, and also between rack units themselves. An accurate estimation of the transient response is therefore essential to achieve a safe pool arrangement and a reliable structural design.

This project has investigated the accuracy of the current analysis methodology, the robustness of the computed outputs and their sensitivity to a number of variables. An assessment of the strengths and weakness inherent to the current analysis methodology has been provided. Implicit assumptions have identified and the major sources of uncertainty related to the input data, modelling properties analysis parameters have been explained in detail. Then, statistical methods for forward uncertainty propagation have been applied to a basic 2-rack system. Transient envelopes and quantitative response surfaces have been built from simulation experiences in ANSYS Mechanical. A multivariate sensitivity analysis has been conducted to assess the influence of the uncertain variables on the numerical outcomes. Latin Hypercube Sampling has been chosen for the design of experiments in order to effectively explore the multidimensional input space. Scatter plots of key variables including seismic and fuel loadings, equivalent dynamic properties, friction coefficients, contact stiffnesses, fuel gaps, inertias, time stepping, convergence tolerances, Rayleigh damping, etc., have been derived. Sobol indices and variance-based importance factors have been obtained from surrogate models computed through Polynomial Chaos Expansions. Finally, a safe design point with the highest probability of failure has been found using reliability methods. Based on these findings, significant recommendations and enhancements of the analysis methodology have been proposed.

6.1 Outcomes

This project has provided a better understanding of the rack seismic analysis covering the following aspects:

- The adequacy of the current analysis methodology, its assumptions, conservatism, weakness, and limits of application;
- The sources of uncertainty coming not only from the stochastic variables, but also from the modelling procedures and the user definition of the analysis controls;
- The uncertainty propagation through the transient analysis and how they affect the stability and robustness of the computed outputs;
- The identification and characterization of relevant variables parameters (input uncertainty);
- The quantification of the global influence of the combination of these uncertainties on the sliding displacements and vertical reactions (output uncertainty);
- The ranking of the governing variables requiring further study;
- The assessment of the probability of failure. Only highly ranked parameters are taken into consideration as uncertain input parameters. This selection is based on a judgment of their influence on the outputs parameter;
- The discussion of the best modeling and analysis methods to develop design guidelines for defining best estimate and conservative analysis;
- Experimental validation/verification of the current analysis methodology;
- The introduction of potential enhancements to upgrade the current methodology.

6.2 Recommendations for future research

This project has been the first attempt to quantify the uncertainty of the rack seismic analysis. Multiple potential sources of uncertainty have been explored assuming wide input distributions to take a macroscopic view of the response surface. Although the analysis has shed light about the rack seismic response and drawn general conclusions about patterns in their behaviour, there is scope to expand beyond the lessons learnt following the directions of research below:

- To increase the accuracy of the surrogate models and its predictive capacity. This investigation has provided surrogates models with reasonably good accuracy. Although the accuracy of the predictions might be further discussed, the shape of the approximated response surface has been considered to be reliable enough. However, there are three possible ways of upgrading these surfaces:
  - Increase the number of simulations of the initial sample. This investigation uses an oversampling ratio (i.e., sample size / minimum sample size) of around 3.
  - Reduce the number of input variables. Screening can be used to reduce dimensionality. Seventeen input variables is a large number and difficult to handle in industrial applications. A refined reliability analysis can be performed focusing only on the governing variables identified in this investigation: friction coefficient, damping ratios, and contact stiffness.
  - Increase the polynomial order of the surrogate model. The latter can resemble the nonlinearities in the rack response better, but can lose accuracy.
- To refine the input distributions. The accuracy of the computed outputs is affected by aleatoric and epistemic uncertainties existing in the input data. The singular nature of the rack seismic problem limits the available information. The water submersion, the radioactive ambient and the low recurrence of earthquakes make difficult to obtain data from on-site measurements or real-condition tests. Here, input data, modelling properties, and solution controls have been considered stochastic. Their probability distributions and range of variation correspond to subjective estimations resulting from expert elicitation, but their confidence is not guaranteed. Further research on the shape of these potential distributions is recommended at least for the next governing variables:
  - Friction coefficients, especially for re-racking projects mixing old and new materials.
  - Impact stiffnesses and allowable penetration.
  - Damping ratios, especially for the water effect and rack shape.
  - Hydrodynamic masses, especially the effect of the presence/absence of outer plates filling the water gaps in-between cells.
- To expand the analysis to:
  - Rack systems of more than two units.
  - Non-symmetric rack systems of more than two units.
  - Rack units connected through upper and lower ties.
- To explore other ways of computing:
  - Damping: Since Rayleigh alpha-damping affects the absolute velocity, it should be discarded if hydrodynamic damping is assumed to be zero. Then, Rayleigh beta-damping is specified to provide a certain damping ratio for a given frequency. This approach generally ensures adequate damping ratios at the lower frequencies, but it causes overdamping of high frequencies (i.e., vertical oscillations and impacts). The use of individual damping elements (type COMBIN in ANSYS) could help to manage the desired damping better.
  - Contacts: The use of elastic contacts requires the specification of uncertain contact stiffnesses with a strong influence on the reaction forces. Alternatively, rigid contacts with a coefficient of restitution can be used. The coefficient of restitution defines the ratio of the relative velocity of rigid bodies after impact to the relative velocity of rigid bodies before impact. Its value varies between 0 (i.e., the rigid bodies stick to each other after impact) and 1 (the rigid bodies rebound after impact with no energy loss).
  - Hydrodynamic masses: A real Computational Fluid Dynamics (CFD) analysis can be performed in order to check the accuracy of the Laplacian flow assumption and the applicability of the thermal analogy. Then, the influence of the turbulent, viscous and sloshing effects can be evaluated..

ACKNOWLEDGMENTS

This project has received funding from the European Union's Horizon 2020 research and innovation programme under the Marie Skłodowska-Curie grant agreement No. 642453.

REFERENCES

[1] Habedank, G., Habip, L.M. and Swelim, H. (1979), 'Dynamic analysis of storage racks for spent fuel assemblies', *Nuclear Engineering and Design* 54(3), 379-383.

[2] Soler A.I. and Singh K.P. (1982), 'Dynamic coupling in a closely spaced two-body system vibrating in a liquid medium: the case of fuel racks' *Proceedings of the 3rd international conference on Vibration in Nuclear Plant*, Keswick, UK.

[3] Soler, A. and Singh K.P. (1984), 'Seismic response of a free standing fuel rack construction to 3-D floor motion', *Nuclear engineering and Design*, 80, 315-329.

[4] Champomier, F., Delemontey, R., Sollogoub, P. and Toumbas D. (1989), 'Seismic design of a spent fuel storage rack', *Proceedings of the 10th International conference on Structural Mechanics in Reactor Technology (SMiRT-10)*, CONF-890855; 589-594, Anaheim, US.

[5] Ashar, H. and DeGrassi, G. (1989), 'Design and analysis of free-standing spent fuel racks in nuclear power plants (an overview)', *Proceedings of 10th International conference on Structural Mechanics in Reactor Technology (SMiRT-10)*, CONF-890855-43, BNL-NUREG-42667. Anaheim, US.

[6] G. DeGrassi, *Review of the technical basis and verification of current analysis methods used to predict seismic response of spent fuel storage racks*, Technical report NUREG/CR-5912, BNL-NUREG-52335, US, 1992.

[7] Zhao, Y., Wilson, P.R. and Stevenson, J.D. (1996), 'Nonlinear 3-D dynamic time history analysis in the reracking modification for a nuclear power plant', *Nuclear Engineering and Design*, 165, 199-221.

[8] Zhao, Y. (1997), 'Finite element modelling and analysis of nonlinear impact and frictional motion response including fluid-structure coupling effects', *Shock and vibration*. 4, 311-325.

[9] Lee, G.M., Kim, K.S., Park, K.B. and Park J.K. (1998), 'Three-dimensional seismic analysis for spent fuel storage rack', *Journal of the Korean Nuclear Society*, 30, 91-98.

[10] Hinderks, M., Ungoreit, H. and Kremer, G. (2001), 'Improved method to demonstrate the structural integrity of high density fuel storage racks', *Nuclear Engineering and Design*. 206, 177-184.

[11] U.S. Nuclear Regulatory Commission, *OT position for review and acceptance of spent fuel storage and handling applications*. Amended by NRC letter in 1979, 1978.

[12] U.S. Nuclear Regulatory Commission, *Standard Review Plan for the review of safety analysis reports for nuclear power plants*, Chapter 3– Design of structures, components, equipment and systems, NUREG-0800, formerly issued as NUREG-75/087, 1981.

[13] US Nuclear Regulatory Commission, *Best-estimate calculations of emergency core cooling system performance*, Regulatory guide 1.157. 1981.

[14] Fujita, K., Tanaka, M., Nakamura, M., Tsujikura, Y. (1988), 'Study of the seismic isolated spent fuel storage rack', *Proceedings of the 9th World conference on Earthquake Engineering*, Tokyo-Kyoto, Japan.

[15] Iwasaki, A., Nekomoto, Y., Morita, H., Taniguchi, K., Okuno D., Matsuoka T. and Chigusa N. (2012), 'Experimental study on free standing rack loading full fuel assembly', *Proceedings of ASME Pressure Vessels and Piping conference (PVP2012)*, 78458, Toronto, Canada.

[16] Kaneko, S. and Shirai, H. (2015), 'Construction of dynamic model for free standing spent fuel rack under seismic excitation', *Proceedings of the Pressure Vessels and Piping conference (PVP2015)*, 45069, Boston, US.

[17] Moudrik, R., Queval, J.C., Gantenbein, F., Champomier, F. and Trollat, C. (1995), 'Test and calculations on a scale one spent fuel storage rack', *Proceedings of conference on Structural Mechanics in Reactor Technology (SMIRT-13)*, Porto Alegre, Brazil.

[18] Queval, J.C, Sollogoub, P., Champomier, F. and Vallat, S. (1999), 'Seismic behaviour of spent fuel storage racks', *Proceedings of Conference on Structural Mechanics in Reactor Technology (SMIRT-15)*, Seoul, Korea.

[19] Sakamoto, K., Kan, R., Takai, A. and Kaneko, S. (2017), 'Construction of dynamic model of planar and rocking motion for free standing spent fuel rack', *Proceedings of ASME Pressure vessels and Piping Conference* (*PVP2017)*, 65172, Hawaii, US.

Chapter 4: Probabilistic analysis of offshore wind turbines: Assessment of operational conditions

Rui Teixeira[1], Alan O'Connor[1], Maria Nogal[1]
[1]Department of Civil, Structural and Environmental Engineering, Trinity College Dublin, College Green, Dublin 2
email: rteixeir@tcd.ie, oconnoaj@tcd.ie, nogalm@tcd.ie

ABSTRACT: This chapter describes work conducted to perform probabilistic assessments of offshore wind turbines towers, while maintaining the focus of the analysis highly related to the current design practices and standards that characterize the design of these systems. Three main fields of analysis are investigated in this context: probabilistic extrapolation of physical quantities, procedures for stress-cycle fatigue design, and meta-modelling of the design procedures. Results from the analysis developed adds new insights to the design of offshore wind turbines, with a particular focus on the tower and substructure components.

KEY WORDS: Offshore wind turbine; Probabilistic analysis; Extreme values; S-N fatigue; Meta-modelling; Sensitivity analysis; Kriging models.

1 INTRODUCTION

The demand for renewable energy is indisputable. Global climate trends have been stimulating the urge to develop low carbon-footprint technologies. Wind energy is one of the most promising alternatives to the conventional energy conversion, which use fossil fuels. While the enthusiasm around the wind energy started in the 1980s, offshore wind only became highly relevant later in the 2000s, with the understanding of the true potential of the resource. The fact that wind depends on the solar rays that reach the Earth set it as a virtually infinite source of energy. The offshore wind energy market has been experiencing exponential growth since the start of the present century. In particular, during the last ten years, the increase in the installation of offshore wind energy was highly relevant. It is accepted that the sectors growing trend is foreseen to continue; however further growth of the sector demands the establishment of more complex and accurate engineering design practices. Reliable operation is a characteristic of major importance in the sector. In the case of Offshore Wind Turbines (OWT), the role of engineering practices and procedures and its relation to the increase of technical competitiveness is remarkable.

IRENA [1] report that innovation has been a key driver for competitiveness in the wind energy sector. Furthermore, they state [2] that research, along with regulatory frameworks, is expected to have a major influence on the OWT development up to 2050. Within this framework, there is high demand for the improvement of the techniques applied in the sector. Such development is expected to unlock breakthroughs that will enable wind energy to become more competitive. At the same time, there is scope for novel practices to unlock breakthroughs in the sector. Figure 1 shows that, despite the significant recent developments, the Levelized Cost of Energy[1] (LCOE) of offshore wind installations is only now achieving the level of economic competitiveness of the most conventional technological ways of converting energy (e.g., those that use fossil fuels). Wind, nonetheless, is among the most widely available renewable resources on Earth.

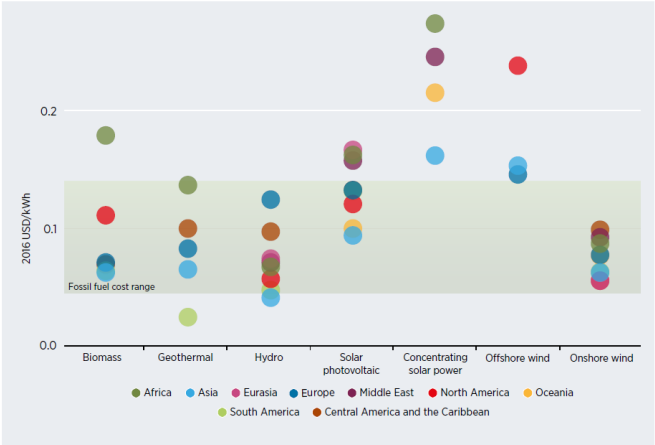

Figure 1. Levelized Cost of Energy (LCOE) for different sources of renewable energy divided by region. Source: [2].

The direct scale-up of wind turbines has been the major driver of economic competitiveness in the sector of offshore wind energy. Larger turbines allow owners to install more capacity and to access a larger resource. The direct benefit of the scale-up is the possibility to amortise the project development costs faster. The increase of the OWT tower height has been a major enabler of competitiveness through the decrease of the LCOE for wind turbines [2].

The fact that the technology to harness the wind energy has converged and is well established allows the sector to compete through directly increasing the dimensions of the technology. It is noted, however, that the scale-up reflects on increasingly challenging engineering designs.

[1] A ratio that includes the operational lifetime costs and divides it by the benefit of energy production.

As the sector advances, an area that has demanded particular concern is the requirement to address uncertainty in the design phase. Better uncertainty characterization practices and understanding enables the establishment of robust and optimized designs. For the designer, uncertainty characterization unlocks a new dimension of comprehension. Perception of the potential deviations experienced by the design variables enables a more complete understating of the risk associated with the operation of an OWT.

Characterizing uncertainty in the design phase is usually enabled by probabilistic analysis. Application of probabilistic analysis to OWT is not a new practice. A brief overview of the standards for designing OWTs (IEC 61400 class) or some recommended guidelines, such as DNV guidelines [3,4], shows that assessing uncertainty is a recurrent process inside the OWT design chain. Nevertheless, and as highlighted earlier, a persisting requirement in the sector is to improve the present design techniques progressively, and to implement new procedures that address uncertainty, where it is not yet accounted for.

Regarding OWT structural performance, some of the turbines' components are not allowed to fail. Less important components are expected not to, but may yet fail. This fact sets two levels of relevance for the system's survivability and per component, critical and non-critical for the overall system survival. Components that are critical for survivability enclose most of the OWT cost breakdown. These are usually structural key elements, commonly with larger dimensions, such as the blades or the tower. Failure in one of these is very probable to result in total loss of the system. BVG report [5] that blades and the tower alone enclose more than 40% of the costs for a 6 MW turbine. The turbines alone, according to [2], comprise 64 to 84% of onshore wind energy projects costs and 30 to 50% of offshore wind energy project costs. Within this breakdown, foundations may account for 1/5 of the project's total cost.

Optimization and improvement during the design phase of these components demand a full understanding of their response. The motivation for the presented work is therefore to discuss some of the design methodologies that intervene in the design of these critical components, with a particular focus on probability techniques and uncertainty characterization. The research conducted is applied to the tower component. Nevertheless, the discussion is extended to how the methods presented and discussed may be applied to other components.

Uncertainty characterization is many times hindered by the large costs needed to perform it. The existing design procedures for OWT are already highly expensive concerning the amount of effort demanded their implementation. Uncertainty characterization increases these design requirements exponentially. Uncertainty characterization, which is intrinsically related to probability theory, addresses repeatability of the design procedure up to a number of times were the designer may be confident that he/she comprehends the problem in-hand and the different uncertainties that affect it. This may range from a simple comparison with observed data to analysis of the results consistency and repeatability. Through efficient characterization of uncertainty, further increase of competitiveness for the OWT sector may be achieved. This is not limited to economic competitiveness, but can also extend to performance. Uncertainty, though, is a broad and wide field of analysis and affects every single design step. Developments on uncertainty assessment have been steadily occurring through small contributions from multiple authors that spend significant efforts in order to comprehend what the sources of error are for each of these steps. Aligned with this, the work described in this chapter adds new insights to the fields of OWT analysis and uncertainty characterization.

2 OBJECTIVES AND CONTRIBUTION TO KNOWLEDGE

Three main global objectives are developed under the framework. The first two objectives relate directly to the design techniques. The third goal is proposed to answer to the demand for procedures that enable designs to be optimized, i.e., cutting the significant cost associated with some of the present design practices. These, presented in-line, are outlined below in an early stage of the research through the identification and tackling of different gaps in the knowledge.

- Extrapolation of physical quantities: The need to extrapolate physical quantities to lengths of time much larger than the available data is a probabilistic problem that concerns multiple fields of knowledge. Usually, a data-set, if available for design, may cover a few years. However, the designer of an engineering project is required to design a structure to survive periods of time much larger than the reference period of time of the data used to undergo design calculations. Situations are rare where long data-sets are available.
- Uncertainty based on probabilistic procedures: The simple fact that a probabilistic procedure is applied does not necessarily contribute to more accurate and robust designs. Design recommendations for OWTs enclose multiple probabilistic techniques that try to characterize uncertainty; extrapolation is only an example of such techniques.
- Effort reduction for design procedures: The cost of some design procedures may hinder design optimization. In such cases, the computational cost required for optimization is too large for the necessary number of iterations required to be performed. Optimization is then implemented using a series of assumptions that enable it to become practicable.

One final consideration that is of major relevance for new implementations in the OWT sector is to relate all the discussed topics with the current design practices. None of the discussions aforementioned are valid if they are not contextualized in the light of the present design procedures. The following sections discuss in more detail the contributions from this work, which is further extended in published research [6-13], structured in order to answer the presented objectives.

3 CHARACTERIZATION OF EXTREME WAVES

The analysis of *exceedance* data is a very efficient alternative to deal with extreme values. Extreme values, as mentioned, are of difficult characterization due to their scarcity. If the availability of data is a limitation, the difficulty of characterizing extreme values is accentuated. The Peak-Over-Threshold (POT) is an efficient alternative to model extreme occurrences due to its capability of enclosing more data in the analysis than similar alternatives that extrapolate physical quantities. There are different stages in the analysis of data with

the POT. A threshold level *u* needs to be defined in first place. This *u* should be carefully selected depending on the data set. The data is truncated according to *u*, and independence needs to be ensured between the truncated points.

A probability model should be used to assess occurrences in the tail region. Depending on the analysis, different probability models may be used. Commonly, for practical applications, the probability models are recommended *a priori* depending on the physical measures being analysed. These recommendations emerge from previous studies regarding the physical quantity being discussed. If a more accurate analysis is needed, different strategies can be used, such as analysing the fitting. Ideally, if enough data are available for validation, the extrapolation can be compared with a measure of a real occurrence.

Several challenges emerge when applying the POT, such as, how to guarantee the independence of the data, what probability models to use, and how to compare them. A comprehensive discussion of these is presented in [13].

3.1 In-field data

In-field data were collected in four buoys located around the Irish coast by Met Éireann. The period of the collection comprised an interval of time of 14 years. Data collected is applied in a comparative study on the procedure to define extreme waves in the design phase. This analysis is motivated by the lack of consistency in the definition of extreme waves, with particular emphasis on the usage of the Generalised Pareto distribution to characterize extreme waves when applying the POT. The Generalised Pareto is the limit distribution for exceedance data. Nevertheless, recommendations on the characterization of significant extreme waves support the application of the Exponential and two-parameter Weibull distributions in detriment of the Generalised Pareto model.

3.2 Results of significant wave data characterization

Results for the comparative analysis involve using five indicators of fitting in order to compare the three probability models mentioned:

- the Kolmogorov-Smirnov Goodness-of-Fitting (GoF) testing;
- the Anderson-Darling GoF testing;
- the Cramér von-Mises GoF testing;
- Probability-Probability plots; and
- Root-Mean-Square-Error.

A new methodology to calculate the value of *u* is defined and built on the lack of uniformity identified in the current methods to characterize the threshold value. It is assumed that a tail region of a Probability Density Function (PDF) starts in the point where its curvature is maximum positive, conditional on the requirement for the maxima to occur for a value of a *x* higher than the value of *x* corresponding to the peak of the PDF. As a result, at a certain value of *x*, an inflection in the curvature of the PDF will occur motivated by the approach of the tail region. In addition, as *x* increases, it becomes more distant from the bulk of the data. To calculate *u*, the maximum value of the curvature, after the inflection point, is selected. An example of such implementation is presented in Figure 2.

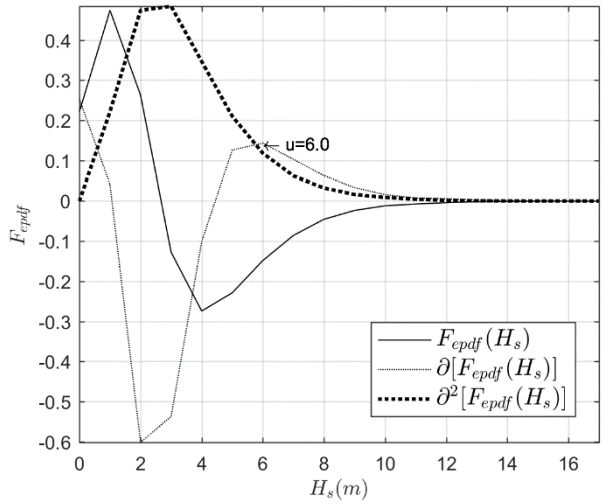

Figure 2. Selection of threshold based on the derivatives of the PDF.

A logarithmic transformation applied to significant wave data is also applied to compute the comparative results on the GoF. It is shown that the logarithmic transformation tends to stabilize the extrapolation with the GP (less variability in the extrapolated value and occurrence of large extrapolated values). This may be connected to the shape parameter that, for the logarithmic transformation, sets the GP to be bounded [13].

Results of the Goodness-of-fit analysis and extrapolation show that there is no evidence to reject the Generalised Pareto distribution over the two-parameter Weibull or the Exponential distributions. The support of the GP distribution and its bounded character is expected to contribute to a more realistic extrapolation of the return level in the physical context of ocean waves. Nevertheless, attention should be given to the selection and fitting process when applying POT to model significant wave *exceedances*. Results also show that when using a POT approach, the user should be careful during the selection of the threshold level that will be used to truncate the significant wave data.

4 COMPARATIVE ANALYSIS OF OWT FATIGUE DESIGN

The present section discusses the application of fatigue time-domain S-N methodologies to design OWT. The IEC Design Load Case 1.2 is selected for a comparative analysis of stress-cycle (S-N) fatigue calculations on the tower component. Different methodologies are accepted to design OWT to fatigue. In regard of S-N fatigue, three main methodologies sre identified:

- direct scale-up of loads and cycles to the design lifetime,
- the statistical fit of the loading distribution, and
- truncation of the tail region.

The methodologies above are compared in the following analysis. The procedure to extrapolate the lifetime fatigue is expected to have a significant influence on the fatigue design results. If a sufficiently representative sample is available for the extrapolation methodology, then fatigue calculations are expected to be accurate. Current practices recommend a minimum of six seeded simulations as a representative sample size at each environmental condition.

Analysis is performed using NREL's baseline turbine mounted on a monopile foundation. Fatigue is assessed at the

base of the tower component, on the Transition Piece (TP) between the tower and the substructure. This is assumed to be the critical loading point for the tower's fatigue response, as it is the location where the bending moment is maximum. Nevertheless, the methods and conclusions presented are valid for any other locations in the tower or even substructure component.

S-N fatigue design of the tower is compared using the following methodologies:

- a 2-parameter Weibull distribution accounting for all loading ranges and fitted using the Maximum Likelihood Estimator (MLE);
- a 2-parameter Weibull distribution accounting for all loading ranges and fitted using the Method Of Moments (MOM);
- truncations at 95% and 99% quantiles (Q) with posterior fit of a Generalised Pareto and a 3-parameter Weibull distribution accounting for the tail of the loading distribution.

In addition to the probabilistic approach, the direct scaling of loads and cycles from the shorter than *T*, *t* time is considered. The comparative analysis performed indicates that the usage of complex estimation techniques is not an adequate substitute for a representative sample for S-N fatigue calculations. The usage of truncation techniques at Q of 95% overestimates S-N fatigue design values. The usage of the whole data-set also overestimates the results. In both cases, a significant error is identified in the approach of large loading amplitude cycles. For large S-N curve slopes, extrapolation is of relevance. For low S-N slopes, the direct scaling of cycles produces the best ratio between the estimation accuracy and the implementation effort.

In order to establish robust design procedures, the comparative approach indicates that the development of an analysis that infers on the uncertainty of the S-N loading spectra is of relevance for S-N fatigue calculations in the tower component. Moreover, in the identified fatigue code calibrations, statistical uncertainty related to the sample size in the definition of loading spectra and consequent approximation of long-term SN fatigue damage or equivalent damage load for *T* is considered in a limited way.

4.1 Bootstrapping to characterize SN fatigue uncertainty

Calculation of confidence intervals (CI) of long-term S-N fatigue using bootstrapping techniques is proposed in order to quantify uncertainty in the assessment of the real long-term S-N fatigue value. The bootstrap is a simple technique to estimate uncertainty in a specified statistic, of particular relevance when limited data is available. Bootstrap has the advantage of being a non-parametric procedure to estimate CI, of particular interest when no assumptions about the data-set are available. Figure 3 presents results for the S-N fatigue mean uncertainty based on bootstrapping of rainflow counting series. Block-bootstrapping is also studied, however it does not contribute for a significant improvement in the accuracy of the results when compared with the less complex empirical bootstrapping.

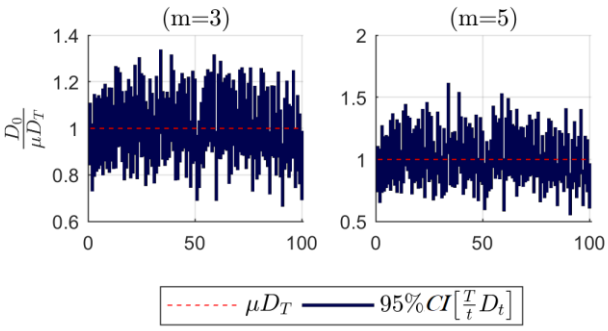

Figure 3. Example of bootstrapping CI intervals for S-N slopes (*m*) of 3 and 5.

5 META-MODELLING FOR OWT S-N FATIGUE CALCULATIONS

It was highlighted that one of the main goals of the work developed is to reduce the effort or the OWT design. Some of the design procedures are identified to be highly resource consuming, inhibiting further optimizations in the design phase. In particular, S-N fatigue calculations are identified to be highly demanding in the design phase. S-N fatigue design procedures demand the assessment of multiple load case scenarios that increase exponentially with the number of variables considered in the problem. This fact limits the application of optimization techniques that consider the full assessment of the S-N structural fatigue. Considering wave states as conditional of the wind parameters is an example of assumptions undertaken to make the fatigue analysis problem manageable.

Meta-modelling is researched as an alternative for efficient fatigue assessments. Meta-modelling has the potential to replace the computationally expensive OWT model and enable a fast and accurate fatigue assessment. In particular, the application of Gaussian process predictors is studied to surrogate fatigue damage. These models have proven before to be efficient surrogates of complex engineering problems. In particular, the Gaussian process predictors, or Kriging models, have presented before the capability to interpolate the response of complex systems efficiently. Kriging regression models emerged recently as powerful tools for reliability and probabilistic analysis due to their capability of interpolating a function and at the same time considering some degree of uncertainty in the interpolation. Kriging models merge the classical regression properties with a local measure of uncertainty, which makes them highly flexible in terms of interpolation. The Gaussian term of $G(x)$ guarantees that a prediction is exactly $g(X)$ at the design of experiments X, even with low order models. In the unknown x space, the interpolation has Gaussian uncertainty.

Being $\boldsymbol{X} = [x_1, x_2, \dots, x_k]$ a vector of realisations of x with respective true evaluations $\boldsymbol{Y} = [g(x_1), g(x_2), \dots g(x_k)]$, $G(x)$, the Kriging approximation, is defined as,

$$G(x) = f(\boldsymbol{\beta}; x) + Z(x) \quad (1)$$

where $f(\boldsymbol{\beta}; x)$ is a deterministic regression model (Equation (2)) with p ($p \in \mathbb{N}^+$) basis function that depends on the order of the regression and that is to be defined based on the $\boldsymbol{X}$

sample; and $Z(x)$ is a Gaussian stochastic process with mean equal to 0 and covariance matrix given by Equation (3).

$$f(\boldsymbol{\beta};\, x) = \beta_1 f_1(x) + \cdots + \beta_p f_p(x) \tag{2}$$

$$\boldsymbol{C}(x_i, x_j) = \sigma^2 R(x_i, x_j; \boldsymbol{\theta}),\ \ with\ i,j = 1,2,3 \ldots k \tag{3}$$

where C defines the correlation generic $\boldsymbol{X}$ points using; the constant process variance σ^2 and a correlation function $R(x_i, x_j; \boldsymbol{\theta})$ that depends on the points and on a set of $\boldsymbol{\theta}$ hyperparameters.

Using the equations above, it can be seen that the fitted surface *G(x)* depends on three main parameters: $\sigma^2, \boldsymbol{\theta}$, and $\boldsymbol{\beta}$. For a set of given support points $\boldsymbol{Y}$, the problem of prediction can be solved through a generalised least squares formulation. One important characteristic of the Kriging interpolator is that $\boldsymbol{Y}$ predictions have a variance component of value 0, meaning the $\boldsymbol{Y}$ is exactly predicted when u takes any value of $\boldsymbol{X}$. It is known that in most cases this does not represent the real behaviour of $\boldsymbol{Y}$ and frequently *g(**X**)* will have some noisy or probabilistic component ε. In such cases, $\boldsymbol{Y}$ is better described by an expected value $\boldsymbol{Y_e}$ and a noise component ε as per Equation (4).

$$\boldsymbol{Y} = \boldsymbol{Y_e} + \varepsilon \tag{4}$$

To account for this effect, a slight modification of the $\boldsymbol{C}(x_i, x_j)$ defined in Equation (3) is introduced in Equation (5).

$$\boldsymbol{C}(x_i, x_j) = \boldsymbol{C}(x_i, x_j) + \boldsymbol{\delta\tau^2} \tag{5}$$

where τ^2 is the vector of the variance of *Y*, the support points used to estimate *G(x)*; and $\boldsymbol{\delta}$ is the identity matrix of size $k \times k$. Figure 4 presents an example of a Kriging model containing a noise component (I) and the same model disregarding it (II).

It is noted that if the goal is to approximate accurately *g(x)*, then the normal interpolator is of interest. In such scenario, the $\boldsymbol{Y}$ prediction is assumed to be perfectly known, and there is no need to introduce further complexity in the model. Using $G(x)$, it is possible to analyse the S-N fatigue using a subset of loading cases that allows to interpolate the response of the system $\forall\, x$.

5.1 S-N fatigue assessment using Kriging models

A search procedure is implemented in order to enable efficient fatigue assessments. It involves three main steps:

- evaluation of the simulation model,
- the definition of the surrogate model and
- S-N fatigue assessment.

Figure 5 presents the methodology implemented to define an accurate $G(x)$. In the figure, the *i* cycle is respective to the search function and number of iterations for it, and *j* is the S-N fatigue sample estimation (number of evaluations to estimate $\boldsymbol{Y}$). The simulation model is jointly analysed with the surrogate model in order to set a surrogate of S-N fatigue design indicators corresponding to the short-term S-N fatigue. The overall goal of the procedure is to replicate the currently recommended design procedure of the IEC61400 series standard.

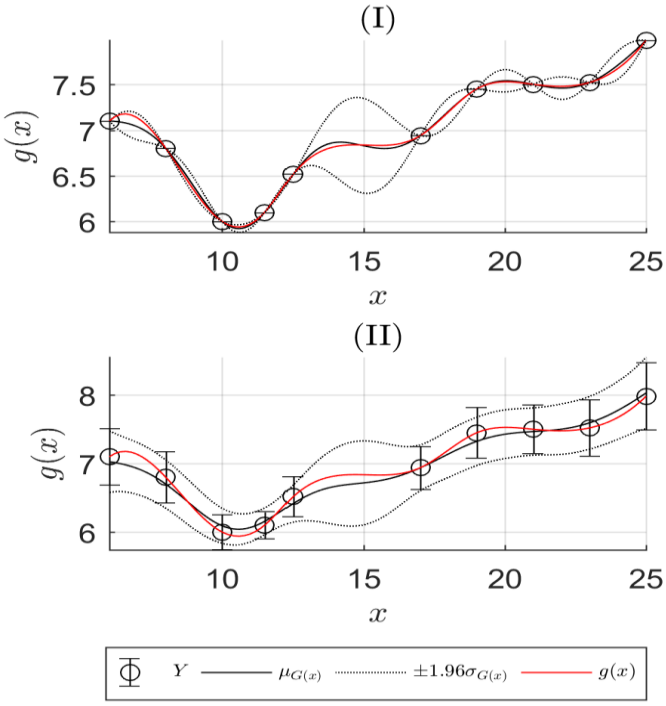

Figure 4. Example of Kriging considering non-noisy **Y** (I) and noisy **Y** (II) for the same **X**.

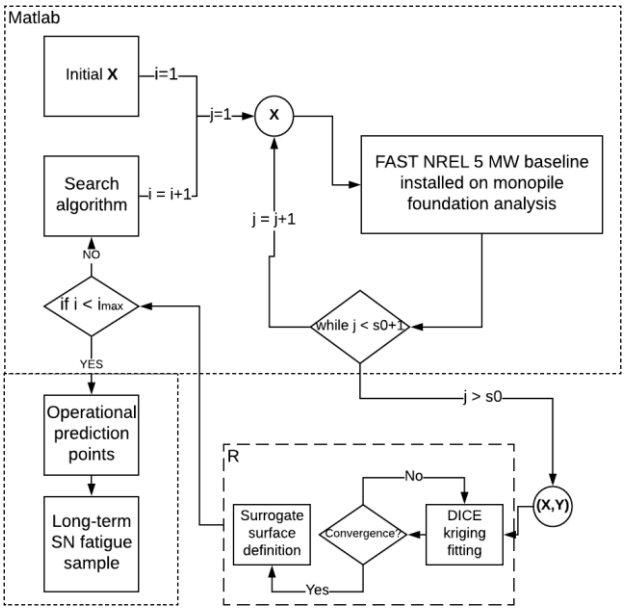

Figure 5. Meta-modelling procedure implemented.

In order to have efficient meta-modelling, it is of interest to have a global comprehension of the problem in hand. Such understanding may allow the efficient allocation of resources during the analysis in the factors of major importance. In the case of complex problems, frequently, if the analysis is not reduced to the variables of major importance, the procedure may become unnecessarily excessive in terms of complexity.

A global sensitivity analysis is developed and is recommended in order to improve the efficiency of the meta-modelling approach. An innovative indicator of probabilistic

sensitivity is introduced with the purpose of developing a sensitivity analysis that also accounts for uncertainty.

5.2 Results of the meta-modelling assessment

A full one-year operation simulation of fatigue is completed in order to validate the results of the meta-modelling approach. The full 1-year simulation comprises 51140 ten-minutes operational simulations of the mentioned OWT model.

An innovative search function that relates to the problem of S-N fatigue is proposed in order to enable accurate S-N fatigue meta-modelling assessments. The meta-modelling results using the innovative search function sre compared with a design of experiments definition using a Latin Hypercube Sampling procedure. The latter is identified to be less robust due to its lower capability to relate to the specificity of the S-N fatigue problem, such as to account for the fact that some operational points comprise significant more S-N damage density than other. Results of the meta-modelling approach sre also compared with the traditional approach that bins environmental data in order to define the operational states where S-N fatigue is assessed.

The effort reduction benefit of using a Gaussian predictor, or Kriging model, as a surrogate of the S-N fatigue damage is identified to be significant. Depending on the allowed error, the computational cost can be cut by a factor of 4 to 10 for m = 3 and 4 to 8, in m = 5. This results in an approximate cut of the design effort time needed to assess S-N fatigue by up to 85% without compromising accuracy. Furthermore, the usage of $G(x)$ to interpolate the short-term S-N fatigue damage allows to interpolate the mean uncertainty. This is achieved using the variance of the estimated mean value. This variance may be used to estimate confidence intervals (CI) in the short-term mean, and long-term mean.

6 CONCLUSIONS

New insights on the operational design for offshore wind turbines and its probabilistic assessment have been presented. For extrapolation of significant wave heights, results of the Goodness-of-Fit analysis and extrapolation have showed that there is no evidence to reject the Generalised Pareto distribution over the two-parameter Weibull and the Exponential distributions. In the case of S-N fatigue, accurate long-term estimations have been seen to depend mainly on the short-term damage estimation loading sample for S-N fatigue calculations. Global sensitivity analysis has been identified to be a powerful tool to decrease the cost needed to solve an engineering problem. Within a complex problem, it is common for only a limited number of variables to comprise for almost all the influence in the problem's output. A meta-modelling technique, using a Kriging surrogate, has been successfully implemented in order to reduce the computational time of OWT S-N fatigue design significantly.

ACKNOWLEDGMENTS

This project has received funding from the European Union's Horizon 2020 research and innovation programme under the Marie Skłodowska-Curie grant agreement No. 642453.

REFERENCES

[1] IRENA, *The power to change: Solar and wind cost reduction potential to 2025*, Technical report, International Renewable Energy Agency, 2016.
[2] IRENA, *Renewable power generation costs in 2017*, Technical report, International Renewable Energy Agency, 2017.
[3] DNV, *Design of offshore wind turbine structures*, Offshore Standard DNV-OS-J101, Det Norske Veritas AS, 2014.
[4] DNV, *Environmental condition and environmental loads*. *Recommended Practice*, DNVRP-C205, Det Norske Veritas AS, 2014.
[5] BVG, *UK offshore wind supply chain: capabilities and opportunities*, Technical report, BVG Associates, 2014.
[6] Teixeira, R., O'Connor, A. and Nogal, M. (2016), 'Comparative analysis of the probabilistic methods to estimate the probability of failure of offshore wind turbine towers', *Proceedings of Civil Engineering Research in Ireland Conference (CERI2016)*, Galway, Ireland.
[7] Teixeira, R., O'Connor, A., Nogal, M., Nichols, J. and Spring, M. (2017), 'Structural probabilistic assessment of offshore wind turbine operation fatigue based on Kriging interpolation', *Proceedings of the 27th European Safety and Reliability Conference (ESREL 2017)*, Portorož, Slovenia.
[8] Teixeira, R., O'Connor, A., Nogal, M., Nichols, J. and Krishnan, N. (2017), 'Analysis of the design of experiments of offshore wind turbine fatigue reliability design with Kriging surfaces', *Procedia Structural Integrity*, 5, 951-958.
[9] Teixeira, R., O'Connor, A. and Nogal, M. (2018), 'Interpolation of confidence intervals for fatigue design using a surrogate model', *Proceedings of New Challenges in Decision Making conference (IFED2018)*, Lake Louise, Canada.
[10] Teixeira, R., O'Connor, A. and Nogal, M. (2018), 'Application of Gaussian process regression for structural analysis', *Proceedings of Civil Engineering Research in Ireland Conference (CERI 2018)*, Dublin, Ireland.
[11] Teixeira, R., Nogal, M. and O'Connor, A. (2018), 'On the calculation of offshore wind turbine load spectra for fatigue design', *Proceedings of the 19th International Colloquium on Mechanical Fatigue of Metals (ICMFMXIX)*, Porto, Portugal.
[12] Teixeira, R., O'Connor, A. and Nogal, M. (2018), 'Convergence analysis for Offshore Wind Turbine operational fatigue reliability analysis'. *Proceedings of the 6th International Symposium on Life-Cycle Civil Engineering (IALCCE 2018)*, Ghent, Belgium.
[13] Teixeira, R., Nogal, M. and O'Connor, A. (2018), 'On the suitability of the generalized Pareto to model extreme waves', *Journal of Hydraulic Research*, 1-16, DOI: 10.1080/00221686.2017.1402829.

Chapter 5: Probabilistic methods for integrated fatigue design and integrity management: fatigue deterioration, crack growth, inspection, and maintenance

Guang Zou[1,2], Kian Banisoleiman[1], Arturo González[2], Michael H. Faber[3]
[1]Global Technology Centre, Lloyd's Register, SO16 7QF, Southampton, UK
[2]School of Civil Engineering, University College Dublin, Belfield, Dublin, Ireland
[3]Department of Civil Engineering, Aalborg University, Aalborg, Denmark
email: guang.zou@lr.org, kian.banisoleiman@lr.org, arturo.gonzalez@ucd.ie, mfn@civil.aau.dk

ABSTRACT: Design and management of welded structural systems against fatigue failures are challenging due to the numerous hot-spot areas involved, uncertainties in deterioration process and maintenance activities, limited available budgets, etc. Traditionally, fatigue design and maintenance decision-making have been disconnected and based on a different theoretical basis, which restricts consistent and optimum decision-making. When the effects of operational maintenance are not quantitatively assessed and considered, design optimization cannot result in the optimum structural plan in terms of Life Cycle total Costs (LCC) and maintenance optimization cannot result in the optimum maintenance plan. This project proposes a risk-based joint decision-making method enveloping major decisions and uncertainties affecting fatigue design, inspection, and maintenance, built upon probabilistic fatigue deterioration modelling, probability inspection modelling, decision tree analysis, and risk-based optimization. Decisions variables in structural scantling and maintenance are simultaneously optimized by risk-based optimization at the initial design stage based on a quantitative assessment of the effectiveness of structural scantling and maintenance interventions. This chapter summarizes essential elements of the proposed method.

KEY WORDS: Integrity management; Probabilistic methods; Fatigue reliability; Fracture mechanics; Inspection; Maintenance.

1 INTRODUCTION

Fatigue is one of the main deterioration mechanisms for welded structural systems under cyclic loading, which compromises structural integrity in the form of crack initiation and propagation. Cracks may initiate at local stress concentration areas or welded details containing initial flaws and then propagate fast under stress ranges. Propagation of cracks can lead to fracture of structural elements and sudden rupture of the whole structural system, e.g., rupture of cross-sections of ships, rupture of a leg causing the collapse of an offshore platform, etc. These failures are often catastrophic, resulting in great losses to owners and operators of assets, not only financially, but also socially and environmentally. Hence, the design and operation of welded structural systems is associated with high risks from fatigue failures.

Structural safety against fatigue is not only an important design consideration, but also a lifetime matter that needs continuing decision-making and measures to mitigate the risks from fatigue cracks. These include safety decisions and measures at the design, construction and operation stage, as given by Figure 1. These decisions are typically made separately and sequentially in current engineering practice.

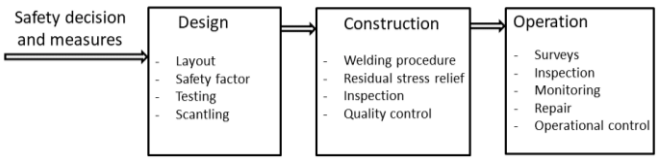

Figure 1. Lifetime safety decisions and measures against fatigue.

Generally, important safety decisions against fatigue are structural scantlings at the design stage, welding and quality assurance techniques at the construction stage and inspection and maintenance programme at the operation stage.

Optimal engineering decision-making against fatigue is often challenged by limited data, knowledge and budgets. It is well-known that fatigue analysis is associated with high degree of uncertainties, originating from inherent variabilities in environmental loads (e.g., wave loads), statistical uncertainties in material properties, inadequate knowledge in the physical process, modelling uncertainties, etc. To support engineering decision-making, numerous studies have been done on fatigue, with analytical, experimental and numerical methods, which contribute to more enriched knowledge on fatigue deterioration and more accurate fatigue analysis methods, including the well-known S-N method [1] and fracture mechanics (FM) method [2]. The S-N method is generally well-stablished and has been adopted widely in designing structures against fatigue, including both deterministic and probabilistic design methods. Based on the FM method, several probabilistic models have been developed to assess reliability [3,4], to update inspection plans based on previous inspection data [5,6], and to develop cost-effective inspection and maintenance plans [7,8] for existing structures experiencing fatigue deterioration. These studies almost exclusively either address fatigue design issues with little quantitative analysis in operational maintenance interventions or address maintenance issues based on given design plans or existing structures.

This project provides a risk-based joint decision-making method enveloping major engineering decisions against fatigue, i.e., design, inspection and repair, and considering failure consequences and sources of uncertainties affecting optimal decisions, as illustrated schematically by Figure 2.

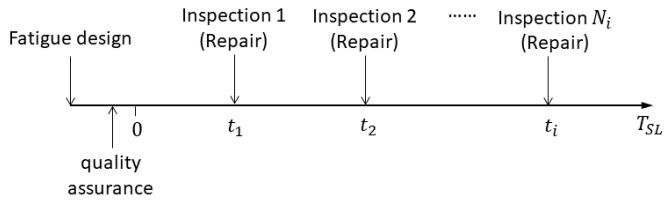

Figure 2. A schematic illustration of joint decision-making against fatigue.

The optimum decision-making problem is addressed by risk-based structural optimization with plate thickness and inspection intervals as optimization variables and solved from an initial design perspective. The method is an expansion of risk-based design optimization to incorporate maintenance variables. The main characteristic of this method is that design, inspection, and maintenance decisions are optimized jointly, as opposed to separately, and thus the effectiveness of safety measures at the design and maintenance stage is fully considered in the initial design decision-making process. As a result, the best compromise between design (and construction) costs and maintenance costs can be achieved, in addition to the best compromise between total structural investments (i.e., the sum of design, construction, inspection and repair costs) and expected failure costs. Another characteristic is that analytical results and then decisions are based on the same probabilistic physical model for fatigue deterioration, and thus, the derived optimum decisions and safety margins are consistent and traceable.

The remainder of this report is organised as follows. Sections 2 and 3 develop two probabilistic modelling methods for fatigue deterioration: the fracture mechanics (FM) and S-N methods and the uncertainties associated with these methods. Section 4 introduces the adopted maintenance strategy, which links the repair decision to inspection result and reviews the models for repair effect on the crack size. Section 5 presents a probabilistic modelling method for inspection quality in terms of crack detection, and the Probability of Detection (PoD) curves for three inspection methods: Magnetic Particle Inspection (MPI), Close Visual Inspection (CVI) and Visual Inspection (VI).

2 PROBABILISTIC FATIGUE MODELLING BASED ON S-N CURVES

Generally, the S-N method is built based on specimen experiments on fatigue life. The fatigue lives of different classes of structural details under different stress ranges and experimental conditions are analysed statistically, and the relationship between fatigue life and stress range is shown by a S-N curve, which characterizes the fatigue resistance of a specific class of structural details.

2.1 S-N curve

Equation (1) gives the formulation of a typical two-segment S-N curve adopted in the marine engineering [9].

$$\begin{cases} N_F \Delta\sigma^{m_1} = \overline{a_1} & N_F \le 10^7 \\ N_F \Delta\sigma^{m_2} = \overline{a_2} & N_F \ge 10^7 \end{cases} \quad (1)$$

where N_F is fatigue life, m_1 and m_2 are the fatigue strength exponents, and $\overline{a_1}$ and $\overline{a_2}$ are the fatigue strength coefficients.

2.2 Fatigue loading

Herein wave loading is considered, as the main source of fatigue loading is cyclic. The stochastics of wave loading can be determined by measurements or direct calculations together with statistical counting methods. It is generally acknowledged that a two-parameter Weibull distribution as in Equation (2) can be used to model the long-term stress distribution reasonably well [9].

$$F(\Delta\sigma) = 1 - \exp\left[-\left(\frac{\Delta\sigma}{q}\right)^h\right] \quad (2)$$

where F is cumulative probability function of $\Delta\sigma$, h is Weibull shape parameter and q is Weibull scale parameter.

2.3 Accumulation of fatigue damage

Miner's rule [10], given by Equation (3), is widely used as an accumulation law for fatigue damage D.

$$D = \sum_{i=1}^{n_b} \frac{n_i}{N_{fi}} \quad (3)$$

where n_i is number of load cycles at the i stress range level; N_{fi} is the fatigue capacity under the i stress range level; and n_b is the number of stress range levels.

Based on Equations (1)-(3), the fatigue damage adopting a two-segment S-N curve for fatigue resistance is formulated by Equation (4).

$$D = N_0\left[\frac{q^{m_1}}{\overline{a_1}}\Gamma\left(1+\frac{m_1}{h};\left(\frac{S_1}{q}\right)^h\right)+\frac{q^{m_2}}{\overline{a_2}}\Upsilon\left(1+\frac{m_2}{h};\left(\frac{S_1}{q}\right)^h\right)\right] \quad (4)$$

where N_0 is the annual number of fatigue loading, Γ is complementary incomplete Gamma function; Υ s incomplete Gamma function; and S_1 is the transition stress range of the two-segment S-N curve.

2.4 Probabilistic analysis

The limit state function based on the S-N method is formulated by Equation (5).

$$h_1 = \Delta - D \quad (5)$$

where Δ is fatigue damage at failure.

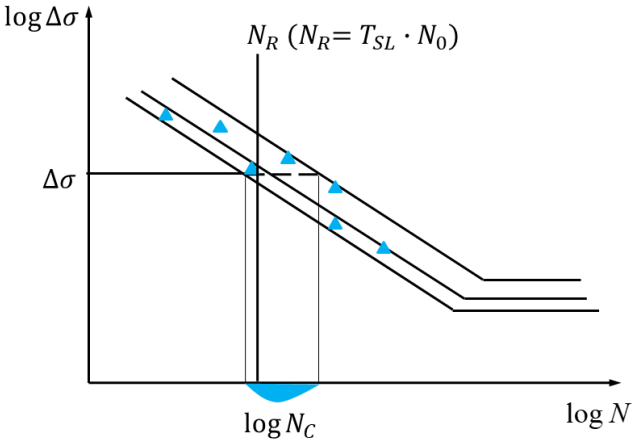

Figure 3. Illustration of fatigue resistance with S-N method.

The main sources of uncertainty associated with S-N methods are uncertainties associated with S-N data (Figure 3), stress range and Miner's rule. It is suggested the use of a bias of 1.0 and Coefficient of Variation (CoV) of 0.3 for the modelling error caused by inaccuracies of the Miner's rule [11]. The uncertainties associated with S-N data are normally indicated in design codes and rules [9].

3 PROBABILISTIC FRACTURE MECHANICS METHOD

The FM method perceives the fatigue deterioration process as the crack evolution from an initial crack size a_0 to a critical crack size a_c, which defines fatigue failure. FM formulations express the relationship between crack growth rate and the local driving force for crack growth. Paris' law [12], given by Equation (6), first relates the crack propagation rate to the range of stress intensity factor.

$$\frac{da}{dN} = C\Delta K^m, \quad \Delta K_{th} \le \Delta K \le K_{mat} \tag{6}$$

where da/dN is crack propagation rate; C and m are material parameters; K_{mat} is material fracture toughness; ΔK is stress intensity factor range; and ΔK_{th} is threshold value for the stress intensity factor range.

The stress intensity factor range ΔK is given by Equation (7).

$$\Delta K = \Delta\sigma Y(a)\sqrt{\pi a} \tag{7}$$

where $Y(a)$ is geometry function and $\Delta\sigma$ is stress range.

The fatigue life during crack growth stage N_P can be obtained by integration of Equation (6) from an initial crack size a_0 to a_c, as expressed by Equation (8). Similarly, the crack size $a(t)$ at time t can be calculated with Equation (9), which is obtained by integration of Equation (6) from the beginning to time t when the accumulated fatigue loading is $N(t)$ cycles.

$$N_P = \frac{1}{\pi^{m/2} C\Delta\sigma^m} \int_{a_0}^{a_c} \frac{da}{a^{m/2} Y(a)^m} \tag{8}$$

$$a(t) = \pi^{m/2} C\Delta\sigma^m \int_0^{N(t)} a^{m/2} Y(a)^m da \tag{9}$$

A limit state function based on crack size is formulated by Equation (10).

$$h_2 = a_c - a(t) \tag{10}$$

A challenge for applying the FM approach is that the resulting crack growth prediction is very sensitive to some input parameters, and that statistical information for the variables is not usually sufficient. Probabilistic methods are recognised to provide a sound theoretical basis for treating both inherent variability and modelling uncertainty.

3.1 Material properties

The fracture parameters C and m are generally seen as material properties, although they are influenced by the environment and loading conditions [11]. The uncertainties in C and m are believed to originate from the inhomogeneities in material, measurement method, procedure and statistical method for parameter estimation. In the probabilistic analysis, C is typically treated as a variable and m is assumed to be constant.

3.2 Stress range and geometry function

The stress range $\Delta\sigma$ and the geometry function $Y(a)$ are very important parameters for crack growth and fatigue life prediction, as they enter the formulation with the power of m. However, detailed calculation of the stress range and geometry function by finite element modelling is often time-consuming. Geometry functions for common welded structural details can be found in [13].

3.3 Threshold of stress intensity factor

The threshold value of ΔK_{th} depends on many factors, e.g., the stress ratio, loading sequence, residual stresses, mean stress, etc. The value $63\ \mathrm{N}\cdot\mathrm{mm}^{-3/2}$ is recommended for welded joints [13]. In this project, the threshold is not considered. The latter is not supposed to induce much inaccuracy, given that the effect of ΔK_{th} on crack growth prediction is small when a value of less than $63\ \mathrm{N}\cdot\mathrm{mm}^{-3/2}$ is employed [14]. The threshold is not considered in the S-N approach either.

3.4 Initial crack/flaw size

The initial crack/flaw size is dependent on the material, the environment, and the welding technique used to construct a structural detail and represents the initial damage state of the structural detail. The distribution of initial crack size is normally obtained by sampling and measuring the maximum crack size of details constructed with similar materials and techniques.

3.5 Failure criteria and the critical crack size

The fatigue life and reliability results are not very sensitive to a small change of the critical crack size, due to the fact that the crack develops very quickly at the final fracture stage, as shown schematically by Figure 4.

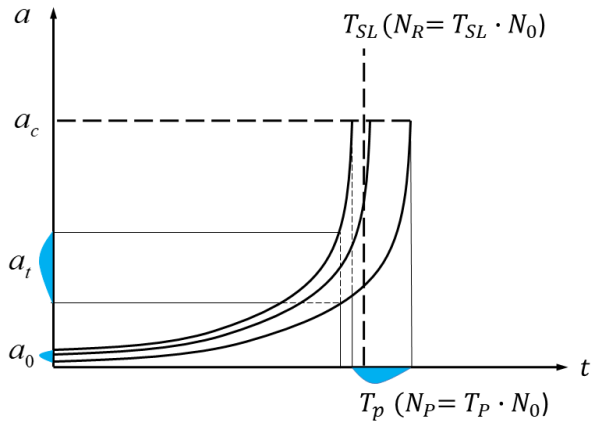

Figure 4. Illustration of fatigue resistance with the fracture mechanics (FM) method.

In one-dimensional crack growth analysis, the critical crack size is often set to be equal to the thickness of the structural element, as the consequence of fracture failure is typically negligible before through-thickness crack occurs. In this project, the critical crack size is also set to be equal to the plate thickness.

4 MAINTENANCE STRATEGY AND REPAIR EFFECT

At the operation stage, it is the repair (or replacement) activities that ultimately improves fatigue reliability and thus mitigates failure risks. Planned inspections and maintenance can improve fatigue reliability only when a maintenance strategy, linking repair actions to inspection results, is specified. Generally, a maintenance strategy defines the condition(s) to carry out repair, e.g., repairs are carried out following negative inspection results and exceedance of repair criteria.

With a maintenance strategy, inspection and maintenance activities can be modelled, and their benefits in terms of risk reduction and associated costs can be assessed quantitatively at the decision-making stage, based on which the optimum inspection and maintenance variables are derived.

The main objective of this project is to develop a risk-based decision-making method considering fatigue design, inspection and repair from an initial design perspective, and to investigate the benefit of joint decision-making compared to separate decision-making. So, complex maintenance strategies are not pursued herein. A detection-based maintenance strategy, under which a repair is carried out upon crack detection by inspection, is adapted to both joint and separate decision-making. The detection-based maintenance strategy is a simple version of condition-based maintenance strategies. However, the risk-based joint decision-making method introduced in Section 5 is able to accommodate other maintenance strategies. Different maintenance strategies can be modelled similarly using decision tree analysis as introduced in Section 5 and incorporated into the joint decision-making method. Optimization methods for maintenance strategies have been addressed by [7,8], and these studies are compatible with the joint decision-making method developed herein.

Widely-used repair methods for cracks in structural engineering include:

- Drilling a hole at the front of a crack;
- Re-welding;
- Re-welding plus post-weld treatment;
- Replacement;
- Grinding.

When these repair methods are applied, they will change the structural system physically, e.g., removing cracks, decreasing the crack size, stopping or slowing down crack growth, etc; and thus change structural performance and fatigue reliability. To quantify the benefits of planned maintenance interventions in terms of risk reduction, it is necessary to assess the effect of a repair on lifetime failure probability. In this project, the safety margins are defined based on crack size, so the effect of a repair is assessed in terms of crack size. The same repair method and the same repair effect model are assumed to be used in a lifetime. It is thought that after a repair, the crack size of a structural system is brought to its initial level, as illustrated by Figure 5, i.e., the distribution of the crack size after the repair is the same as the initial crack size a_0. This repair effect model has been adopted widely by studies on probabilistic maintenance optimization [6-8]. Other more sophisticated repair effect models include the repair effect model based on deterioration rate [15], the 'as bad as old' model [16], random repair effect models [17], etc. However, these repair effect models generally require more computational efforts when integrated into probabilistic optimization methods, and their applications have been very limited. Also, for high integrity structures, the probability of repair is very low, particularly when strict repair criteria are adopted. Hence, the influence of the repair effect model on the lifetime failure probability and eventually on the optimum inspection and maintenance decisions is small for high integrity structures.

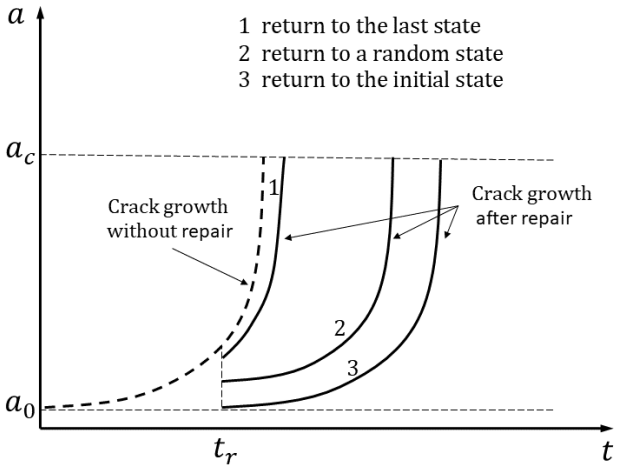

Figure 5. Illustration of models of repair effect on crack size.

5 PROBABILISTIC INSPECTION MODELLING

Under a condition-based maintenance strategy, inspections are carried out to provide new information on crack damage states, in addition to initial probabilistic crack growth prediction with the Paris law, both of which provide decision basis for repair. Typical inspection methods used in structural engineering include VI, CVI, Non-Destructive Testing (NDT) methods, e.g., MPI, ultrasonic testing, acoustic emission inspection, and Structural Health Monitoring (SHM) techniques.

There are uncertainties associated with any inspection method and the performance reliability of an inspection method needs to be quantified before the benefits of planned inspection and maintenance activities in risk reduction can be assessed. The detectability of an inspection method is probabilistic inherently, as many factors can influence inspection results. It is often found that the indication of an inspection cannot reveal the true damage states. In addition, the detectability of an inspection method is influenced by the training and knowledge of inspectors. Generally, the inspection result depends on the reliability of the specific instrument-human system. The following factors contribute to variabilities in inspection results:

- The characteristics of a crack, such as its shape and size;
- Human factors associated with an inspector;
- The procedure of carrying out an inspection;
- The specific instrumentation;
- The environments in which an inspection is carried out.

The reliability of an inspection instrument-human system is often adequately characterized based on the concept of PoD, so that the accuracy level provided by an inspection result can represent the true crack characteristics and the confidence level on inspection results can be demonstrated. The PoD is defined as the probability of a given crack with a fixed size to be detected by a given inspection method. PoD curves are typically obtained by inspection experiments on structural

details containing a range of crack sizes. Based on experimental results, an appropriate function is assumed for the PoD curve, and coefficients of the function are estimated by statistical methods. Confidence range on the PoD function can also be specified based on the estimated coefficients. However, the experimental approach is usually costly and time-consuming, since there are so many factors that can affect the probability of detection and need to be tested. In this project, the exponential PoD function given by Equation (11) is employed.

$$PoD(a) = F(a) = 1 - \exp(-a/E(a_d)) \quad (11)$$

where $E(a_d)$ is the mean detectable crack size.

With the above function, uncertainties associated with inspection performance are addressed by modelling the detectable crack size a_d of an inspection method as an exponentially distributed variable. The PoD function is equal to the Cumulative Density Function (CDF) of the variable a_d. Three inspection methods are investigated: MPI, CVI, and VI. The PoD curves associated with these methods are presented in Figure 6.

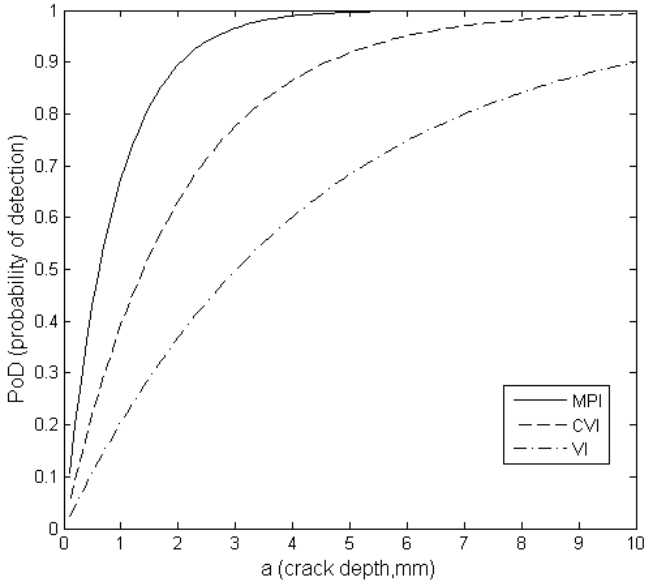

Figure 6. Probability of detection (PoD) curves for three inspection methods.

It is of great interest to consider the influence of inspection uncertainty in maintenance optimization because the benefits and costs of maintenance are affected by inspection decisions (inspection times and methods), which are subjected to inspection uncertainty. However, the influence of inspection uncertainty on maintenance optimization has not been explicitly and adequately covered in the literature. With each inspection method the max reliability indexes corresponding to the PoD functions associated with inspection uncertainty (i.e,, Figure 6) and perfect inspection (i.e., inspection uncertainty is not considered) are derived. Equation (12) defines the effectiveness of a planned inspection.

$$\eta = \beta'_{iu,max} / \beta'_{pi,max} \quad (12)$$

where $\beta'_{iu,max}$ is the max lifetime reliability under the scenario 'inspection uncertainty'; $\beta'_{pi,max}$ is the max lifetime reliability under the scenario 'perfect inspection', i.e., inspection uncertainty is not considered.

Figures 7 gives lifetime reliability index against planned inspection time for the CVI method using typical normal distributions from the literature for the variables of the FM crack propagation model. As expected, the max lifetime reliability index generally decreases when inspection uncertainty is considered for all the three inspection methods. η values of 0.908, 0.913 and 0.972 are obtained for VI, CVI and MPI respectively. When considering inspection uncertainty, the effectiveness of a planned inspection adopting MPI is higher than adopting CVI and VI. If an inspection is scheduled at the late stage of service life, inspection uncertainty has little influence on the lifetime reliability index. If an inspection is scheduled at the early stage of service life, the lifetime reliability index can be higher when inspection uncertainty is considered than neglected in the case of adopting CVI or VI.

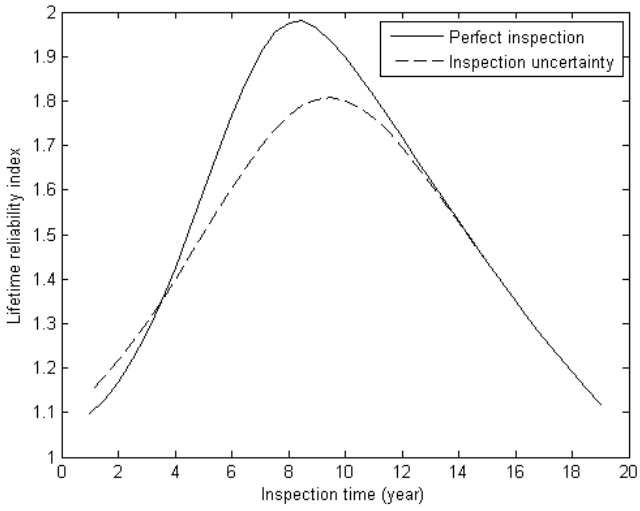

Figure 7. Lifetime reliability index against inspection time (CVI).

6 CONCLUSIONS

Welded structural systems are susceptible to fatigue primarily due to the presence of initial flaws, among other factors. Structural reliability against fatigue and fracture failures are lifetime considerations which require decisions on, e.g., plate thickness, allowable stress range, welding quality assurance procedure, inspection intervals, repair method, etc. In current practice, the structural fatigue design and structural integrity management are generally disconnected, i.e., integrity management optimization has not received due considerations in the design stage, and integrity management optimization is done at the operational stage when the structural plan can hardly be changed.

With a holistic perspective, this project has developed a risk-based method for jointly optimizing design and maintenance plan for structures subjected to fatigue. The method has been developed using probabilistic modelling of fatigue damage accumulation, crack growth, inspection quality, and effect of repair. The method is able to model the combined effects of structural geometry and maintenance strategy on the lifetime fatigue reliability and costs.

ACKNOWLEDGMENTS

This project has received funding from the European Union's Horizon 2020 research and innovation programme under the Marie Skłodowska-Curie grant agreement No. 642453.

REFERENCES

[1] Lassen, T. and Recho, N. (2009), 'Proposal for a more accurate physically based S– N curve for welded steel joints', *International Journal of Fatigue*, 31(1), 70-78.
[2] Cui, W., Wang, F. and Huang, X. (2011), 'A unified fatigue life prediction method for marine structures', *Marine Structures*, 24(2), 153-181.
[3] Ayala-Uraga, E. and Moan, T. (2007), 'Fatigue reliability-based assessment of welded joints applying consistent fracture mechanics formulations', *International Journal of Fatigue*, 29(3), 444-456.
[4] Feng, G.Q., Garbatov, Y. and Guedes Soares, C. (2012), ' Fatigue reliability of a stiffened panel subjected to correlated crack growth', *Structural Safety*, 36–37, 39-46.
[5] Chen, N.-Z., Wang, G. and Guedes Soares, C. (2011), ' Palmgren-Miner's rule and fracture mechanics-based inspection planning', *Engineering Fracture Mechanics*, 78(18), 3166-3182.
[6] Dong, Y. and Frangopol, D.M. (2016), 'Incorporation of risk and updating in inspection of fatigue-sensitive details of ship structures', *International Journal of Fatigue*, 82, 676-688.
[7] Kim, S., Soliman, M. and Frangopol, D.M. (2013), 'Generalized Probabilistic Framework for Optimum Inspection and Maintenance Planning', *Journal of Structural Engineering*, 139(3), 435-447.
[8] Soliman, M., Frangopol, D.M. and Mondoro, A. (2016), 'A probabilistic approach for optimizing inspection, monitoring, and maintenance actions against fatigue of critical ship details', *Structural Safety*, 60, 91-101.
[9] DNVGL-RP-0005, *Fatigue design of offshore steel structures*, Det Norske Veritas AS, Oslo, Norway, 2016.
[10] Miner, M. (1945), 'Cumulative Damage in Fatigue', *Journal of Applied Mechanics*, 12(3), A159-A164.
[11] DNVGL-RP-0001, *Probabilistic methods for inspection planning for fatigue cracks in offshore structures*, Det Norske Veritas AS, Oslo, Norway, 2015.
[12] Paris, P. and Erdogan, F. (1963), 'A critical analysis of crack propagation laws', *Journal of basic engineering*, 85(4), 528-533.
[13] BS7910, *Guidance on methods for assessing the acceptability of flaws in metallic structures*, British Standards Institution, London, 2000.
[14] Lotsberg, I. and Salama, M.M. (2010), 'Crack propagation versus crack initiation lives of FPSO weld details', *Proceedings of the ASME 29th International Conference on Ocean, Offshore and Arctic Engineering, American Society of Mechanical Engineers*, Shanghai, China.
[15] Zhou, X., Xi, L. and Lee, J. (2007), 'Reliability-centered predictive maintenance scheduling for a continuously monitored system subject to degradation', *Reliability Engineering & System Safety*, 92(4), 530-534.
[16] Doyen, L. and Gaudoin, O. (2004), 'Classes of imperfect repair models based on reduction of failure intensity or virtual age', *Reliability Engineering & System Safety*, 84(1), 45-56.
[17] Zhang, M., Gaudoin, O. and Xie, M. (2015), 'Degradation-based maintenance decision using stochastic filtering for systems under imperfect maintenance', *European Journal of Operational Research*, 245(2), 531-541.

Chapter 6: Residual life assessment and management of ship unloaders

Giulia Milana[1,2], Kian Banisoleiman[1], Arturo González[2]
[1]Lloyd's Register, Global Technology Centre, Southampton, UK
[2]School of Civil Engineering, University College Dublin (UCD), Dublin, Ireland
email: giulia.milana@lr.org, giulia.milana@ucdconnect.ie, kian.banisoleiman@lr.org, arturo.gonzalez@ucd.ie

ABSTRACT: This chapter provides an overview of the research carried out on ship unloaders. Having identified the dynamics of these structures as a critical element when assessing the remaining fatigue life, transient dynamic analyses are carried out on the most representative structural element, i.e., the lifting boom. Within an unloading cycle, two main phases are identified: travelling of the moving system and hoisting of the payload. Using an equivalent finite element of the lifting boom, dynamic analyses are carried out modelling the two aforementioned phases. The influence of parameters, such as travelling/hoisting speed and acceleration, on the dynamic response is considered. In addition, the maximum total (static + dynamic) response from simulations is compared with the response obtained applying an amplification factor to the static analysis following guidelines from standards. Furthermore, the simplified model of the lifting boom is used to estimate some parameters, such as the mass of the payload or the distance at which the moving system stops, which are commonly not recorded when acquiring data from the monitoring system, but relevant towards a fatigue life assessment. Fatigue life is then calculated using the missing parameters estimated on-site, and compared with the results of a conventional procedure to highlight the advantages of allowing for a more accurate estimation of stress ranges.

KEY WORDS: Ship unloader; Fatigue; Dynamics; Moving load; Hoisting.

1 INTRODUCTION

Ship unloaders represent a crucial link in the maritime transport system. When subjected to continuous hoisting cycles, the structural elements are subject to alternating stresses due to both horizontal and vertical motions. Furthermore, due to the proximity of the sea, they are exposed to an extremely aggressive environment. It is then easy to understand why port cranes are subjected to a rapid rate of deterioration compared with welded structures located in friendlier environments. In general, this deterioration is associated with two cumulative damage processes: fatigue and corrosion. In particular, the most critical effects can be identified as a loss of thickness due to corrosion and cracks due to fatigue. The consequences derived from fatigue cracking are of a major relevance, even in the case in which they do not lead to complete failure, in terms of safety and costly inspections and repairs. Towards the end of the life of a ship unloader, maintenance becomes more expensive and the impact on their productive capacity is more serious. For this reason, the definition of a detailed maintenance program assessing the remaining life of existing ship unloaders can lead to a significant reduction of risk and cost associated with unexpected failures.

1.1 The structure

It is possible to identify many different types of cranes depending on their structural layout, lifting capacity or application. Among them, grab ship unloaders are selected here. The main aim of these large-scale port cranes is unloading bulk materials from ships to the hopper, from where they are then taken to the storage yard through a conveyor belt. The common scheme of a generic grab ship unloader is shown in Figure 1.

Figure 1. Structural elements of a ship unloader.

1.2 Structural monitoring

The experimental data employed in this project comes from the continuous monitoring of a ship unloader during two weeks when unloading of different vessels takes place. The structure is a 34-year-old grab ship unloader, located in Scotland, used to unload coal. The monitoring system, represented by 48 channels of strain, was installed at 16 locations, in a full bridge configuration [1].

The graph in Figure 2 shows the variation in vertical bending stress for the north side of the lifting boom for a single

unloading cycle (approximately 55 seconds). It is possible to identify three main phases:

1) the trolley, with the empty hanging grab, is travelling from above the hopper to the lifting boom;
2) the trolley is fixed at one location on the lifting boom, while the empty grab is lower, filled and then lifted; and
3) the trolley, with the full grab, is travelling back to the initial position, to release the payload.

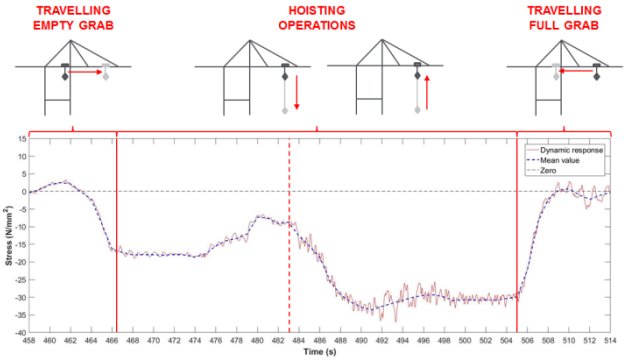

Figure 2. Single unloading cycle and identification of main phases (vertical bending stress for north side lifting boom).

2 RESEARCH OBJECTIVES

Since failure on a crane or its components would have catastrophic consequences in terms of both fatalities and economic impact, due to an unscheduled interruption in service and maintenance operations, it is vital to prevent these failures by investigating their causes and carrying out an accurate assessment of the remaining life of these structures. An outcome an initial literature review is that the main causes of failures can be grouped into four categories that are:

- overloading and wear;
- material defects;
- corrosion;
- fatigue.

This project has paid attention to fatigue [2], since the consequences related to fatigue cracks are a main threat to the safety of these structures. Therefore, the main aim of this research is to reduce the uncertainties affecting the evaluation of fatigue life of a ship unloader, to achieve a more accurate assessment of these structures and consequently to reduce the risk and cost associated with unexpected failures. Figure 3 shows the standard procedure for fatigue life assessment that has been identified on completion of the state of art review and the main areas covered by this project in order to increase the accuracy of this process (in red in Figure 3). These aspects will be presented in detail in the following sections.

3 DYNAMIC ANALYSIS

For comparison purposes, a transient dynamic analysis is carried out following the standards. As shown by Figure 3, the standard procedure is based on a pseudo-static analysis combined with the introduction of dynamic amplification factors.

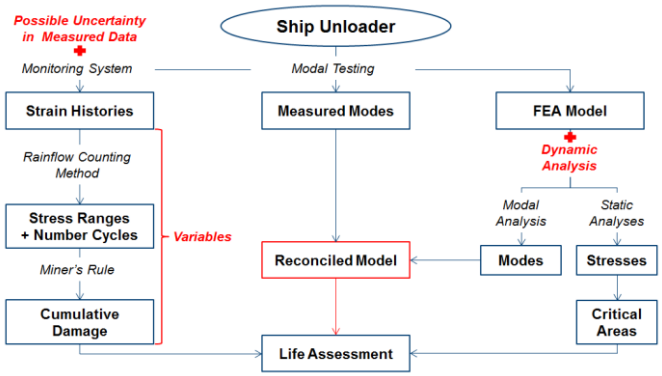

Figure 3. Standard procedure for fatigue life assessment.

For example, FEM 1.001 [3] suggests using a dynamic coefficient, ψ, to be applied to the working load, in order to take into account, the variation due to the picking up of the load, acceleration, and deceleration of the hoisting motion as well as the travelling. Furthermore, for the specific case of hoisting an unrestrained grounded load, a number of standards [3-5] suggest to replace the aforementioned coefficient with a more conservative amplification factor, ϕ_2, to take into account the transferring of the load from the ground to the crane, given by:

$$\phi_2 = \phi_{2,min} + \beta_2 \cdot v_h \quad (1)$$

where $\phi_{2,min}$ and β_2 are two variables defined as a function of the hoisting class, while v_h is the steady hoisting speed in m/s.

Ship unloaders are slender structures with relatively low frequencies, which make them prone to dynamic excitation. Since the latter can considerably shorten their fatigue life, a dynamic analysis is required to achieve a more accurate assessment of the structure. Thus, transient dynamic analyses are carried out to investigate the dynamic response of the structure and to then identify the influence of each parameter on the response. The general equation governing the problem is given by:

$$[M]\{\ddot{u}\} + [C]\{\dot{u}\} + [K]\{u\} = F(t) \quad (2)$$

where $[M]$, $[C]$ and $[K]$ are the global mass, damping and stiffness matrices of the FE model, respectively, and $\{\ddot{u}\}$,$\{\dot{u}\}$ and $\{u\}$ are the respective acceleration, velocity and displacement DOFs.

Results from solving the equation of motion are compared with a baseline case obtained applying the standards' guidelines are provided. Both travelling and hoisting phases are analysed.

3.1 Travelling phase

The problem of a moving load has been a topic of growing interest in structural engineering, initially related mainly to the response of bridges and then extended to machines, such as cranes, heavily involved in the construction industry. In the case of cranes, the problem is generally brought back to the case of a simply supported beam [6-8]. In a few cases, a more suitable model was adopted, for example in Zrnic et al [9], in which an equivalent mathematical model of the lifting boom is introduced. They solve the problem of a moving load

analytically, considering only the case of a moving mass [9]. The model proposed by Zrnic et al [10], presented in Figure 4, is the basis for carrying out a comprehensive study of the dynamic response due to the travelling and the hoisting operations using the Finite Element (FE) method. The finite element model of the lifting boom is coded in MATLAB. It consists of 22 Euler beam elements of three-meter-length, for a total length of 66 m. Three degrees of freedom are considered for each node (x, y and θ) to take into account both longitudinal and transversal displacements.

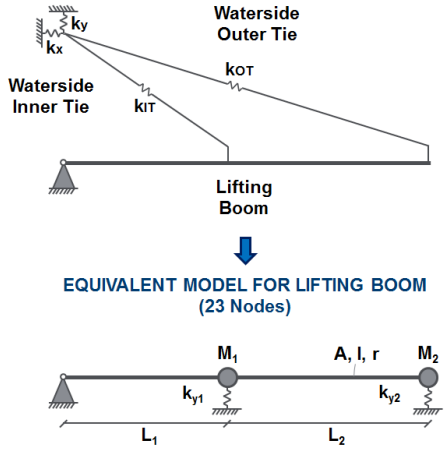

Figure 4. Equivalent finite element model of the lifting boom, adapted from Zrnic et al [10].

The beam is pin-joined at the left-hand side, at the location at which the lifting boom is connected to the central boom in the real structure. The lumped masses (M_1 and M_2) are due to the waterside weights while the two vertical linear springs (K_{y1} and K_{y2}) introduce in the system the stiffness of the upper substructure, except for the boom. The first three natural frequencies of the FE model resemble those values provided by Zrnic et al [10], with a maximum difference in natural period of 0.54% (Table 1).

Table 1. Comparison natural frequencies for the first three modes

	Built model	Literature (Zrnic et al [10])	Comparison
Mode	T (s)	T (s)	Error (%)
I	0.6879	0.6860	0.27
II	0.3120	0.3108	0.39
III	0.1186	0.1180	0.54

Figure 5 shows the different ways in which the moving system (composed by the trolley, the grab, and the payload) is modeled. From left to right-hand side, the models presented are a moving point load, a moving mass, a moving sprung mass, a moving two sprung masses and finally a pendulum. Apart from the moving point load, in all other cases, the interaction between the moving system and the structure is taken into account, resulting in time-dependent matrices of mass, stiffness, and damping. In addition, the fact of the moving system travelling along a deflected beam is modelled including coriolis and centripetal forces in the equations of the problem. Different speed patterns are considered in order to investigate the influence of braking and acceleration on the dynamic response of the structure.

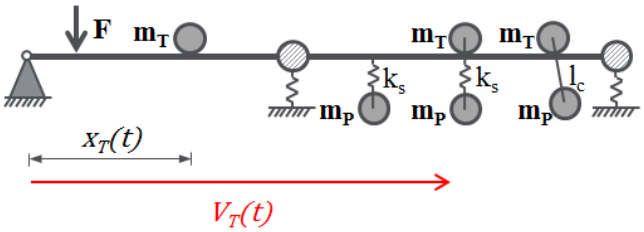

Figure 5. Different ways of modelling the moving system, composed by the trolley, the grab and the payload.

Figure 6 shows the dynamic response in terms of vertical displacement at the first spring location for each model when travelling at a constant speed V_T, of 6 m/s, in comparison with the static response. Additional cases and comparisons are referred in [11].

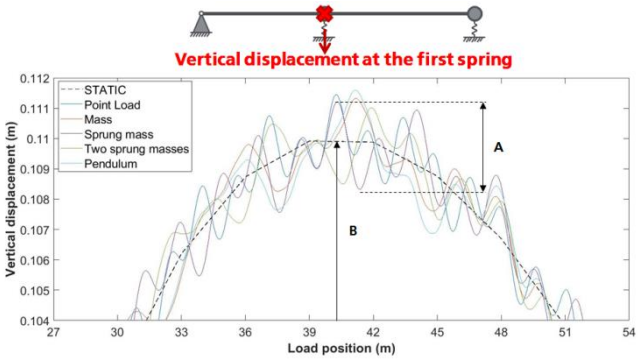

Figure 6. Dynamic response in terms of vertical displacements for all the moving system models considering a constant travelling speed of 6 m/s.

It can be seen (Figure 6) that, for the maximum achievable speed in real life operations (6 m/s), the dynamic response is very close to the static one. If a term denoted as Dynamic Response Factor (DRF) is defined as:

$$DRF = \frac{dynamic\ peak\ to\ peak\ (A)}{static\ response\ (B)} + 1 \quad (3)$$

the values obtained are shown in Table 2 and below 1.1 for all models considered.

Table 2. Dynamic Response Factor (DRF) values for all the moving system models, with a constant speed of 6 m/s.

Point load	Mass	Sprung mass	Sprung 2 masses	Pendulum
1.017	1.020	1.026	1.023	1.025

3.2 Hoisting phase

Even though the hoisting phase plays a crucial role in the dynamic response of cranes according to the recommendations from standards, this topic has not received much attention in the literature. Conversely, many researchers have focused on the motion due to the payload sway [12-14]. For this reason, the hoisting operation is investigated here through the introduction of a time-dependent force profile. The equivalent

FE model of the lifting boom introduced before is used in combination with the 'sprung two masses' model (Figure 5). The latter takes into account the flexibility of the hoisting system and the oscillation of the payload.

The moving system is assumed to be fixed at the right free end of the beam (Figure 7) while carrying out the hoisting operation, which is the most unfavourable configuration in terms of vertical bending stresses. The initial conditions for the hoisting phase are taken from the final condition (i.e., displacements, acceleration, vertical bending stress) of the travelling phase, considering a final brake that leads to a stop by the right end of the beam.

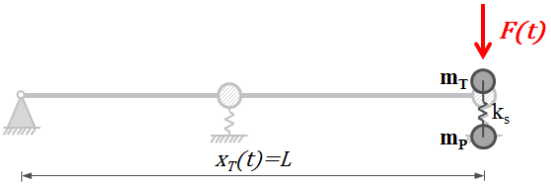

Figure 7. Assumptions made for the investigating the hoisting phase.

The time-dependent applied force $F(t)$ is decomposed in two components: one due to the mass of the trolley $m_T \cdot g$ and one due to the mass of the payload $m_P \cdot a^*(t)$ (Equation (4)).

$$F(t) = m_T \cdot g + m_P \cdot a^*(t) \quad (4)$$

where g is the gravitational acceleration ($9.81\ m/s^2$), $a^*(t)$ is the global vertical acceleration acting on the payload mass m_P , and m_T is the mass of the trolley. While the component due to the mass of the trolley is constant both in amplitude and location, the one due to the payload varies in amplitude. This time-dependency is taken into account through the global vertical acceleration $a^*(t)$. For the latter, three profiles A, B and C, shown in Figure 8, are assumed to calculate the applied force, $F(t)$:

- The profile A is given by a simplified interpretation of the qualitative force profile provided by Section 9.3 of the document FEM 1.001 [3].
- Profile B presents a step in the global vertical acceleration due to a constant hoisting acceleration; it is assumed that when the hoisting operation starts, the initial speed is zero, and it then increases constantly until reaching a constant hoisting speed.
- While these two profiles take variation in the applied force due to both the increase of the payload and the hoisting operations into account, the profile C includes only the increase in the hoisted mass, without including any motion due to the operation.
- A baseline case is established by carrying out the static analysis where the payload is multiplied by the amplification factor, ϕ_2. Assuming a steady hoisting speed of $2\ m/s$, a hoisting class HC3 and an operation method HD5, the value of ϕ_2 in Equation (1) is 1.66.

As shown by Figure 8, the profiles A and B are defined in order to have a peak acceleration equal to the baseline case.

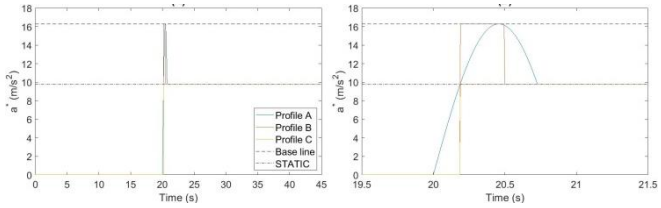

(a) (b)

Figure 8. (a) global vertical acceleration vs time for the acceleration profiles considered, (b) zoomed-in portion of (a).

Figure 9 shows that the response obtained modelling the hoisting operation is much higher than the static response, presented by the dashed line. In order to quantify this scatter, and compare the responses with those obtained from the travelling phase, the DRF is evaluated for each profile as per Equation (3). The values of the factors obtained are 3.15, 2.97 and 2.1 for profile A, B, and C, respectively. Comparing these values with those presented in Table 2, it is possible to appreciate that the hoisting operation plays a dominant role in the dynamic structural response.

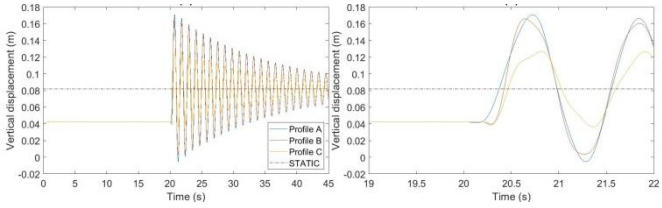

(a) (b)

Figure 9. (a) Vertical displacement at the first spring location for the three force profiles in comparison with the static deflection, (b) zoomed-in portion of the response in (a).

Figure 10 gives the response in terms of vertical bending stresses for the three profiles. It is worth noting that the responses from profiles A and B are very close to each other, which means that the amplification factor provided by the standard can be attributed to the initial phase of the hoisting operation in which there is a constant hoisting acceleration during which the load is transferred from the ground to the crane.

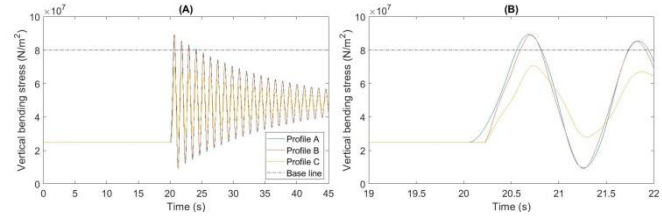

(a) (b)

Figure 10. (a) Vertical bending stress at the first spring location for the three force profiles in comparison with the static deflection, (b) zoomed portion of the response in (a).

Profiles A and B give a maximum response higher than that obtained considering the baseline case; consequently, for the cases analysed the standard does turn out to be conservative. Conversely, when the only variation in the payload mass is taken into account (profile C), the standard is conservative. To quantify these effects, a Dynamic Amplification Factor (DAF) is defined as the ratio of the maximum total (static + dynamic) response to the static response. The DAF values of

displacement are 1.85, 1.85 and 1.46 for profile A, B, and C, respectively. Clearly, dynamic effects due to the initial hoisting operations cannot be ignored. A more detailed description of the profiles A, B and C and their impact on the dynamic response is presented in [15].

4 RECONCILED MODEL OF LIFTING BOOM

Previous analyses are carried out building on a structure found in the literature [10], for which the parameters of the equivalent model (A, I, ρ, M_1, M_2, k_{y1}, k_{y2}) are already defined. In practise, many of these parameters will be unknown. This section employs experimental measurements to adjust the simplified model of Figure 11 corresponding to the monitored structure. Model parameters are determined to resemble the real behaviour of the structure.

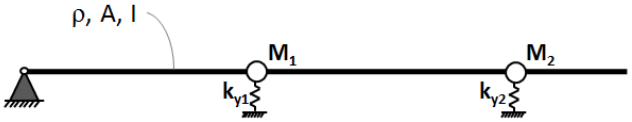

Figure 11. Equivalent model of the lifting boom for the structure investigated.

Initially, a three-dimensional (3D) FE model of the whole structure is built on ANSYS and reconciled with the real measurements in terms of natural frequencies and modal shapes derived from operational modal analysis. Then, the 3D model is used to reconcile the equivalent 2D model of the lifting boom, by minimizing the differences between the two responses. The comparison is carried out in terms of vertical bending stresses (with no gravity) to estimate the two linear stiffnesses (k_{y1}, k_{y2}) and in terms of vertical displacements to evaluate the two lumped masses (M_1, M_2) and the beam density (ρ). An additional verification is completed in terms of natural frequencies and modal shapes. Table 3 gives the values of the parameters obtained after tuning the model.

Table 3. Parameters defining the equivalent 2D model of the lifting boom, for the monitored ship unloader.

A	0.07472 m^2	I	0.02823 m^4
M_1	83424 kg	M_2	122845 kg
K_{y1}	46889940 N/m	K_{y2}	31004370 N/m
ρ	15713 kg/m^3		

5 UNCERTAINTY IN MEASURED DATA

A common source of uncertainty affecting the assessment of a ship unloader is the lack of recorded information when acquiring the data from the monitoring system. This lack of information can result in an over-conservative estimation of the stress ranges affecting the crane members and consequently in unnecessary replacements of structural elements. The values of the stress ranges constitute the starting point for a fatigue life assessment. This section assumes the equivalent model defined in Section 4, to carry out transient dynamic analyses considering a whole unloading cycle. The vertical bending stresses from the 2D model refer to a distance of 27 m from the left pinned end, which corresponds to the location of a transducer on the real structure. Figure 12 shows the variation of vertical bending stresses with time at this location, for a single cycle.

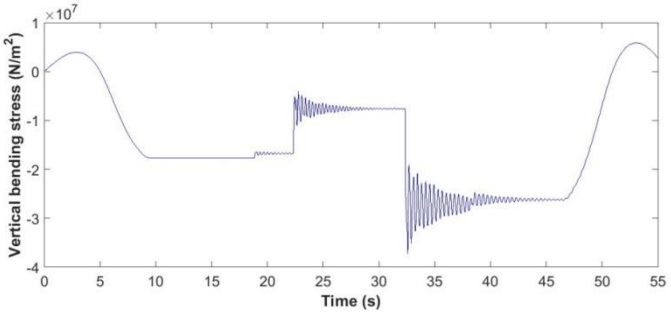

Figure 12. Vertical bending stresses at 27 m from the left pinned end (2D model) for an unloading cycle.

When defining an unloading cycle, twelve variables are identified, i.e., travelling speed and acceleration/breaking, hoisting speed, etc. In order to reduce the number of variables, a sensitivity analysis is conducted and looking at Sobol sensitivity indices, the two most influencing parameters turn out to be the mass of the payload (m_P), and distance from the left pinned end of the beam, at which the trolley stops in order to carry out hoisting operations (x_{stop}). The following analysis is then conducted considering only these two variables and assigning a mean value to the other variables. The simplified equivalent 2D model of Figure 11 is used to obtain a surface response. Figure 13 plots the value of the stress ranges as a function of these two variables.

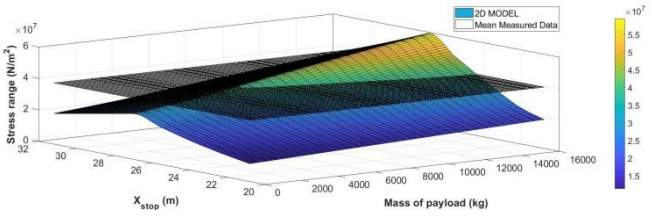

Figure 13. Surface response from the equivalent model of the lifting boom (2D model) and horizontal plane at the mean value of the measured data.

The variables m_P and x_{stop}, are not directly captured by monitoring systems, which are typically more focused on measuring the structural response, but can be estimated from the stress ranges measured in the real structure. The data from the monitoring system (Figure 14(a)) is processed and a Probability Density Function (PDF) identified for the stress range during the monitoring period (Figure 14(b)); the mean value is taken as reference. The latter is also used to intersect the response surface obtained from the 2D model (Figure 13).

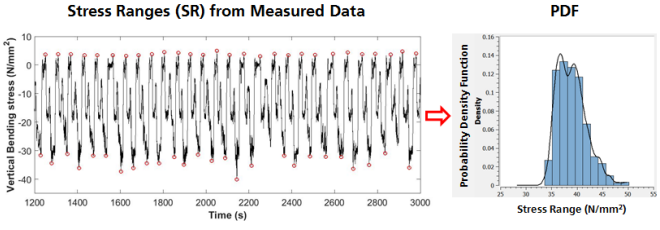

(a) (b)

Figure 14. (a) Sample of the measured stress ranges for the north side of the lifting boom, (b) probability density.

The intersection of the surface, obtained from the 2D model in Figure 13, with the mean stress range from the recorded data, leads to the curve shown in Figure 15. This curve can be used to estimate the mass of the payload once the distance x_{stop} has been evaluated from the travelling phase (x^*_{stop}). For the latter, a similar process is followed, in which the only variable is the distance x_{stop}. At the end of this optimization process based on a response surface methodology, the values of the two variables, x^*_{stop} and m^*_P, giving the mean value of the measured stress range are defined. These parameters can then be used for evaluating, in a more accurate way, the stress ranges at other locations where the monitoring system was not installed.

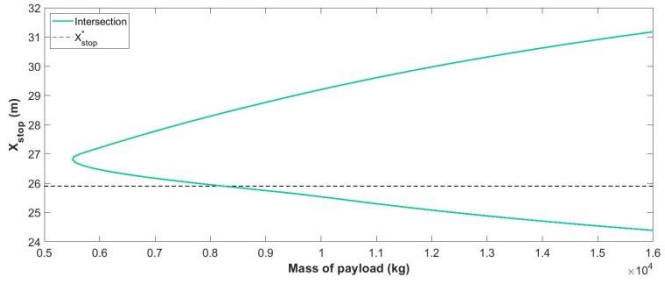

Figure 15. Intersection curve between the response surface from the 2D model and the mean measured data.

5.1 *Application to fatigue life assessment*

The standard procedure for fatigue life assessment assumes x_{stop} equal to the maximum design outreach of the moving trolley and m^*_P equal to the maximum capacity of the grab. In fact, in the absence of recorded information, analysis must be carried out in a conservative way. However, if recorded information was available, two alternative procedures are proposed based on the optimization process presented in the previous section: (*i*) Multiple Stress Ranges (MSR), and (*ii*) Single Stress Range (SSR). Within the first procedure (MSR), the PDF for the stress range is decomposed into a number of stress ranges as shown by Figure 14(b). For each range, using the cumulative density function, the ratio between the number of the cycles completed at that stress range and the total number of cycles is identified. In addition, for each stress cycle, the value of the payload mass is estimated following the procedure explained before assuming the same location x_{stop} for each cycle. Conversely, in the second procedure (SSR) a single stress range using the mean value from the measured data is considered.

A fatigue life assessment is carried out based on S-N curves and Miner's rule for the cumulative damage. Using the 3D FE model of the whole ship unloader, the remaining life is estimated for each structural element. The residual life in terms of remaining tonnes to be lifted is plotted in Figure 16 for the most critical finite elements of the lifting boom. The histogram shows that the standard procedure provides a remaining life that is less than half of that obtained introducing a probabilistic approach based on site-specific data. The standard procedure might lead to an assessment by far over conservative, while a more accurate representation of the load applied to the structure and of the unloading cycle, can avoid unnecessary replacements.

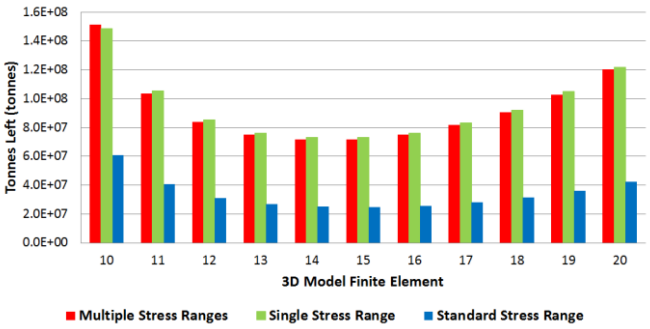

Figure 16. Remaining tonnes applying the three fatigue life assessment procedures to the most critical 3D model finite elements of the lifting boom.

6 CONCLUSIONS

This project has investigated the impact of the travelling and hoisting operations on the dynamic response of the lifting boom of a ship unloader. The lifting boom has been used to carry out transient dynamic analysis, since it has been recognized to be the single most representative element in the dynamic response of these structures. The response of the lifting boom is the result of two components interacting with each other: the underlying structure (representing the waterside portion of the boom), and the applied load. During the travelling phase, the applied load has been modelled as a moving point load, a moving mass, a moving sprung mass, a moving two sprung masses and a pendulum point load. During the hoisting phase, the load has been modelled using different force profiles and a baseline based on pseudo-static analysis. The dynamic impact of the travelling phase has been proven to be very small compared to the impact of the hoisting phase regardless of the load model being employed. Following a sensitivity analysis, the parameters that mostly influence the total stresses of the structure during a loading cycle, and hence fatigue life, have appeared to be the payload mass and the distance at which the trolley stops to carry out hoisting operations. Alternative fatigue life assessment procedures have been proposed to take these site-specific conditions into account.

ACKNOWLEDGMENTS

This project has received funding from the European Union's Horizon 2020 research and innovation programme under the Marie Skłodowska-Curie grant agreement No. 642453.

REFERENCES

[1] Milana, G., Banisoleiman, K. and Gonzalez, A. (2017), 'Field characterization of location-specific dynamic amplification factors towards fatigue calculations in ship unloaders', *Proceedings of 27th European Safety and Reliability Conference (ESREL2017)*, Portoroz, Slovenia.

[2] Milana, G., Banisoleiman, K. and Gonzalez, A. (2016), 'Sources of structural failures in ship unloaders', *Proceedings of 26th European Safety and Reliability Conference (ESREL2016)*, Glasgow, UK.

[3] F.E.M. 1.001, *Rules for the design of hoisting appliances*, 3rd edition revised 1987.10.01, Federation Europeenne de la Manutention, 1998.

[4] BS EN 1991-3:2006, *Eurocode 1 - Actions on structures, , Part 3: Actions induced by cranes and machinery*, British Standards Institution, 2006.

[5] BS EN 13001-2:2004+A3:2009, *Crane safety-General design-Part 2: Load effects*, British Standards Institution, 2011.

[6] Gasic, V., Zrnic, N., Obradovic, A. and Bosnjak, S. (2011), 'Considerations of moving oscillator problem in dynamic responses of bridge cranes', *FME Transactions*, 39, 17-24.
[7] Oguamanam, D.C.D., Hansen, J.S. and Heppler, G.R. (1998), 'Dynamic response of an overhead crane system', *Journal of Sound and Vibration*, 213(5), 889-906.
[8] Oguamanam, D.C.D., Hansen, J.S. and Heppler, G.R. (2001), 'Dynamics of a three-dimensional overhead crane system', *Journal of Sound and Vibration*, 242.
[9] Zrnic, N.D., Hoffmann, K. and Bosnjak, S.M. (2009), 'Modelling of dynamic interaction between structure and trolley for mega container cranes', *Mathematical and Computer Modelling of Dynamical Systems*, 15(3), 295-311.
[10] Zrnic, N.D., Oguamanam, D.C.D. and Bosnjak, S.M. (2006), 'Dynamics and modelling of mega quayside container cranes', *FME Transactions*, 34, 193-198.
[11] Milana, G., Banisoleiman, K. and González, A. (2018), 'Impact of a moving trolley on the dynamic response of a ship unloader boom', *Proceedings of 13th International Conference on Steel, Space and Composite Structures, (SS18)*, Perth, Australia.
[12] Yazid, E. (2011), 'Mathematical modeling of a moving planar payload pendulum on flexible portal framework', *Journal of mechatronics, electrical power, and vehicular technology*, 2, 99-104.
[13] Marinovic, I., Sprecic, D., and Jerman, B. (2012), 'A slewing crane payload dynamics', *Technical Gazette*, 19.
[14] Jerman, B., Podrzaj, P. and Kramar, J. (2004), 'An investigation of slewing-crane dynamics during slewing motion-development and verification of a mathematical model', *International Journal of Mechanical Sciences*, 46, 729-750.
[15] Milana, G., Banisoleiman, K. and Gonzalez, A. (2018), 'Characterization of hoisting operations on the dynamic response of the lifting boom of a ship unloader', *Proceedings of The sixth International Symposium on Life-Cycle Civil Engineering (IALCCE 2018)*, Ghent, Belgium.

The TRUSS project (www.trussitn.eu) has received funding from the European Union's Horizon 2020 research and innovation programme under the Marie Skłodowska-Curie grant agreement No. 642453